

INTERDIGITATED MICROELECTRODES FOR BIO-SENSING APPLICATIONS

by

DU WANG

A THESIS

Submitted in partial fulfillment of the requirements
for the degree of Master of Science in the
Applied Optics Graduate Program
of Delaware State University

DOVER, DELAWARE

May 2019

This thesis is approved by the following members of the Final Oral Review Committee:

Dr. Mukti Rana, Committee Chairperson, Division of Physical and Computational Sciences,
Delaware State University.

Dr. Mohammad Khan, Committee Member, Division of Physical and Computational Sciences,
Delaware State University.

Dr. Jun Ren, Committee Member, Division of Physical and Computational Sciences,
Delaware State University.

Dr. Jinjie Liu, External Committee Member, Division of Physical and Computational Sciences,
Delaware State University.

DEDICATION

This thesis is dedicated to my family for their endless love beyond the years.

ACKNOWLEDGEMENT

I would like to express my sincere appreciation to my supervisor Dr. Mukti Rana for his valuable supervision and dedicated academic training provide to me. Without his vision and constant help this study would not have been possible. I would specially like to show my great appreciation to Dr. Murali Temburni and Dr. Dual Man, for their expertise in electroporation and kindly help me set up the experiment.

I am highly indebted to Ms. Jacquelyn J.Jones for the financial assistance she provide to me. Thanks my undergraduate supervisor Dr. Deborah Santamore for giving me the research opportunities and motivating me to keep exploring in graduate study. Besides that, I would also like to express my thanks to my supervisory committee members - Dr. Jun Ren, Dr. Jinjie Liu and Dr. Mohammad Khan for their precious time examining my work.

I would like to thank my wife Siting Lyu for her consistent support and great patience provided to me whenever I needed.

I would also like to acknowledge the financial, academic and technical support for this research from the College of Agriculture Science and Technology, Optical Science Center for Applied Research and its staff. I wish to express my gratitude to all the colleagues and lab members for their excellent collaboration and kind support. Thanks to my fellow worker Nicholas Calvano for his help on equipment setting in my research lab. I would like to thank Christiane Ebongue for inviting me to join the SPIE student Chapter at Delaware State University and help me to become an officer of the Chapter.

Finally, I want to thank all the individuals helped me in past two years of my graduate study at DSU. It had been a wonderful time and I love the activities that I had at DSU graduate student life.

Interdigitated Microelectrodes for Bio-sensing Applications

Du Wang

Faculty Advisor: Dr. Mukti Rana

ABSTRACT

According to the data from Centers for Disease Control and Prevention, Salmonella (*S. typhimurium*), a common food borne pathogen, is responsible for more than one million illnesses each year in the United States alone. It is one of the top most pathogens contributing to domestically acquired foodborne illnesses resulting in 19,336 hospitalizations and 386 deaths per year. The annual cost, directly and indirectly, associated with food-borne illness, is estimated to be around \$77 billion a year. Most food poisoning is caused by the toxins produced by the bacteria or by the bacteria themselves. Once the food is placed in a humid and warm environment, certain bacteria can grow from one to millions in a very short periodic. Identification and detection of this food-borne pathogen is one of the keys to reduce the outbreak caused by this. Most of the conventional methods available for separation and detection of salmonella use specific agar media to separate and count bacterial cells in particular samples. These detection techniques consist of multiple steps and sub-processes which are often time consuming and take 3-4 days for initial results and up to 6-7 days for confirmation. Though these methods provide reliable data, they are not suitable for scenarios where rapid detection is the key.

This work presents the design and simulation of an alternating current-DEP (Dielectrophoresis) field flow fractionation (DEP-FFF) type microfluidic chip which will detach the target cells of *S.*

typhimurium from complex mixed culture solution with high efficiency. For design and simulation of the device, microfluidic channels were created on Silicon wafer and interdigitated electrodes were built in to apply the electric field (and DEP force) on the target cells. In addition to *S. typhimurium*, other unknown cells (two bacteria) were added to from the mixed solution. The design and simulation process was done by using various modules of finite analysis software - COMSOL Multiphysics. The physical dimensions of the microfluidic chip (length, depth and width) was varied to see the effect of these on cell separation efficiency. For target cells of *S. typhimurium* the cell separation efficiency was found to be ranging between 80.5% to 95.1%.

Electroporation is one of the most efficient ways to transfect primary cells with minimum adverse effects compared to all other available technologies. As part of this work, electroporation of the cells for DNA transfer was done without damaging the cells. For this purpose, an *in situ* nanofiber-electroporation chip was developed to deliver DNA into hard-to-transfect cells, especially primary neuronal cells. The *in-situ* electroporation chip was composed of interdigitated metal electrodes lines and a biocompatible nanofiber membrane on a cover glass substrate. Metal electrodes made of Au were fabricated using liftoff technique on the cover glass substrate in the cleanroom. PCL nanofiber membrane was electropun and was aligned with the electrodes. The chip system provided conducive cell growth environment, and enabled the cells get transfected while the cells adhered during the electroporation. The transferred cells were inspected under the fluorescence microscope after electroporation is done.

Table of Contents

LIST OF TABLES	x
LIST OF FIGURES	xi
CHAPTER I.....	1
1.1 Background and Motivation.....	1
1.2 Conventional Pathogen Detection Methods.....	2
1.2.1 Polymerase Chain Reaction	3
1.2.2 ELISA Assay	4
1.3 Sensor Based Pathogen Detection Methods.....	5
1.3.1 Impedance	5
1.3.2 Microfluidic Activated Pathogen Detection.....	7
1.4 Outline of this Thesis	7
CHAPTER II	9
2.1 Microfluidic Lab-on-a-chip	9
2.2 Dielectrophoresis.....	9
2.2.1 Single Membrane Spheres Particles.....	10
2.2.2 Single Membrane Ellipsoids Particle	12
2.2.3 Alternative Current-Dielectrophoresis	13
2.3 Dielectrophoresis Based Microfluidic Chip.....	14
2.3.1 Non-field flow fractionation(FFF).....	15
2.3.2 Field flow fractionation (FFF)	17
2.3.3 Gravity involved FFF	20
2.3.4 DC-DEP FFF.....	20
CHAPTER III.....	22
3.1 Electrical Properties of Pathogens.....	22
3.2 Design and Simulation of the Microfluidic Chip	23
3.2.1 Parameters and Constant Values	24
3.2.2 Geometry Build.....	25
3.2.3 Addition of Physics Module	27
3.2.4 Study	30
CHAPTER IV	31
4.1 Clausius-Mossotti Factor	31
4.2 Separation Process.....	36
4.3 Device Modeling	41
4.4 Separation Result for zone 1 of the Device	42
4.5 Separation Result for zone 2 of the Device	48
CHAPTER V.....	53
5.1 Result Analysis.....	53
5.2 Conclusion	55
5.3 Summary	56
5.4 Future Work.....	56

CHAPTER VI	58
6.1 Introduction	58
6.2 Fundamental Principles	58
6.3 Electroporation Chip	59
6.3.1 Electroporation Chip Design	59
6.4 Fabrication Process	60
CHAPTER VII	64
7.1 Cell Preparation	64
7.2 Chip Preparation	65
7.3 Electroporation	65
7.4 Result	66
7.5 Conclusion and Future Work	66
References	68

LIST OF TABLES

Table 1-1: Food-borne illness caused by different pathogens in several counties.....	2
Table 3-1: Parameters and variables used in simulation.....	24
Table 4-1: Measured dielectric constant for four different bacteria under ambient and dry conditions.....	32
Table 4-2: Performance of device with 10000 μm length and 240 μm width, while the channel depth varied between 20 μm to 50 μm	46
Table 4-3: Performance of device with 10000 μm length and 20 μm depth, while the channel width between 200 μm to 320 μm	47
Table 4-4: Performance of device with 240 μm width and 20 μm depth, while the channel length varied between 8000 μm to 15000 μm	47
Table 4-5: Performance of device with 10000 μm length and 240 μm width, while the channel depth between 20 μm to 50 μm	51
Table 4-6: Performance of device with 10000 μm length and 20 μm depth, while the channel width between 200 μ to 320 μm	52
Table 4-7: Performance of device with 240 μm with and 20 μm depth, while the channel length between 8000 μm to 15000 μm	52
Table 5-1: Recent DEP separation chip application.....	55

LIST OF FIGURES

Fig. 1-1: Schematic diagram of polymerase chain reaction process.....	4
Fig. 1-2: Conceptual view of impedance-based microfluidic detectors.....	6
Fig. 2-1: Schematic diagram of non-uniform electric field and induced particle.....	11
Fig. 2-2: Schematic diagram of an ellipsoids particle.....	12
Fig. 2-3: Schematic illustration of the DEP force acted on the dielectric particles.....	14
Fig. 2-4: Design for a DEP separation chamber.....	15
Fig. 2-5: The separation of mixed viable and nonviable cells.....	16
Fig.2-6: Schematic of a continuous cell separation chip using hydrodynamic DEP.....	18
Fig. 2-7: Schematic views of microfluidic chip with electrodes array generated on the side wall.....	19
Fig. 2-8: Side view of the camber and the force diagram of the particle.....	20
Fig. 2-9: DC-DEP particle separation chip using triangular hurdle with divergent output branches.....	21
Fig. 3-1: Schematic diagram of a bacteria.....	22
Fig. 3-2: Operation window for COMSOL Multiphysics.....	23
Fig. 3-3: Geometric modeling window of OMSOL Multiphysics.....	26
Fig. 3-4: AD/DC physics module and its component.....	27
Fig. 3-5: Creeping flow physics module and its component.....	28
Fig. 3-6: Particle tracking for fluid flow.....	29
Fig. 3-7: Study options for COMSOL Multiphysics.....	30
Fig. 4-1: CM factor for pathogens with different permittivity.....	33

Fig. 4-2: CM factor for pathogens with different conductivity.....	35
Fig. 4-3: 2D separation device.....	36
Fig. 4-4: Separation process for the testing device at different frequencies.....	38
Fig. 4-5: Top view of the micro fluidic channel.....	42
Fig. 4-6: Schematic of the zone 1 of the microfluidic device.....	43
Fig. 4-7: Separation process in part 1 of the device.....	45
Fig. 4-8: Schematic of the zone 2 of the microfluidic device.....	48
Fig. 4-9: Separation process in zone 1 of the device.....	50
Fig. 5-1: Schematic diagram of how particles attracted by positive DEP force and stick on the electrode arrays.....	54
Fig. 6-1: Layout of the photomask containing 32 different designs of electrode lines.....	60
Fig. 6-2: Steps of photolithography process.....	61
Fig. 6-3: An illustration of lift-off process.....	62
Fig. 6-4: Photograph of an actual chip aligned with PCL nanofiber.....	63
Fig. 7-1: GFP plasmids is delivered into using the electroporation chip and expressed in chicken embryo optic-tectum cells.....	66

CHAPTER I

INTRODUCTION

1.1 Background and Motivation

In United States, there were about 47.8 million food-borne illnesses per year. The annual cost, directly and indirectly, associated with food-borne illness, is estimated to be around \$77 billion a year. Most food poisoning is caused by the toxins produced by the bacteria or by the bacteria themselves. Once the food is placed in a humid and warm environment, certain bacteria can grow from one to millions in a very short periodic. The more bacteria, the higher the chance of infection and illness. The most common bacteria that cause the infection are *Campylobacter jejuni*, *Salmonella* and *Escherichia coil* [1,2]. For each food-borne bacteria, the incubation period varies. Some cause symptoms within 30 minutes to hours, and most food-borne illness cases develop symptoms after 12-48 hours. Other types of food-borne diseases do not appear until a few days to a week later. The most common symptoms of food-borne illness are vomiting, abdominal pain and diarrhea caused by inflammation of the gastrointestinal tract (stomach and intestines). Symptoms also include fever and chills, bloody stools, dehydration, myalgia, weakness and exhaustion, depending on the cause of food-borne illness. In some extreme cases, food-borne diseases can be very serious, leading to damage to the nervous system. In extreme cases, it even leads to paralysis or death. Prevention of microbial-induced food-borne illnesses is a huge challenge for food safety department in various countries due to the diversity of sources of pollution as shown in Table 1-1.

Table 1-1: Food-borne illness caused by different pathogens in several counties [3]

PATHOGEN	PERCENTAGE FOOD-BORNE (%)					
	WHO (2015)	USA (2011)	Canada (2015)	Australia (2005,2014)	England and Wales (2002)	Netherlands (2008)
<i>BACILLUS CEREUS</i>	100	100	99	100	100	90
SHIGA-TOXIN-PRODUCING <i>ESCHERICHIA COLI</i> (STEC)	40-60	68	61	56	63	40
<i>SALMONELLA</i> NON-TYPHOIDAL	46-76	94	63	72	92	55
<i>SHIGELLA SPP.</i>	7-36	31	26	12	8	NE
<i>STAPHYLOCOCCUS AUREUS</i>	100	100	78	100	96	87

Because food safety issues have brought enormous challenges to human society, a rapid separation and detection of bacteria has always been a hot topic of research. Till today, there are various pathogen detection techniques have been reported to prevent the spread of the food-borne illness [4,6,8,10]. Based on the different principle, they can be divided into two categories: conventional and sensor-based methods.

1.2 Conventional Pathogen Detection Methods

Traditional bacterial detection methods are often based on identifying some of the biochemical properties of the bacteria themselves. At very beginning, streaking is a common method to isolate the bacteria. By inoculating mixed bacteria into a culture plate, repeated streaking, dilution and

culture, pure strains were obtained from the plate. Beside streaking, there are still couple of conventional methods to detect pathogens such as: the polymerase chain reaction method (PCR) [4] and the enzyme-linked immunosorbent assay (ELISA) [5]. Because it takes a lot of time to prepare the culture environment, proliferate bacteria and identify features, therefore, these methods are cumbersome to operate and usually takes more than a week to get the test results [6].

1.2.1 Polymerase Chain Reaction

PCR is a technique established by K. Mullis in the late 1980s to promote the amplification of specific Di-oxi Nucleic Acid (DNA) segment by polymerase in vitro [4]. PCR requires a pair of specific oligonucleotide primers designed for the target gene and then uses the target gene as a template to amplified the specific DNA sequence. Since the reaction cycle can be performed a certain number of times, a large amount of the gene of interest can be amplified in a short time. PCR technology has the characteristics of high sensitivity, strong specificity and easy operation.

Fig. 1-1 illustrate the cycling process of polymerase chain reaction. The standard PCR process is divided into three steps, and the conversion of each step is controlled by the change in temperature. The first step is denaturation in which double-stranded DNA template cleaves hydrogen bonds in a heated reaction chamber (94°C-96°C) and breaks into two single-stranded DNA. The next step is to anneal the reaction temperature around 65°C. During this time, the primer will attach on the 3' end of each single-strand DNA. The last step is extension, by reheating the reaction chamber to a proper temperature - 72°C for thermus aquaticus (Taq) polymerase. Under the action of Taq DNA polymerase, the dNTPs were added from the reaction mixture to synthesizes a new DNA strand from 5' to 3'. This cycling process is repeated to allow rapid amplification of the target DNA [7-9].

Polymerase chain reaction - PCR

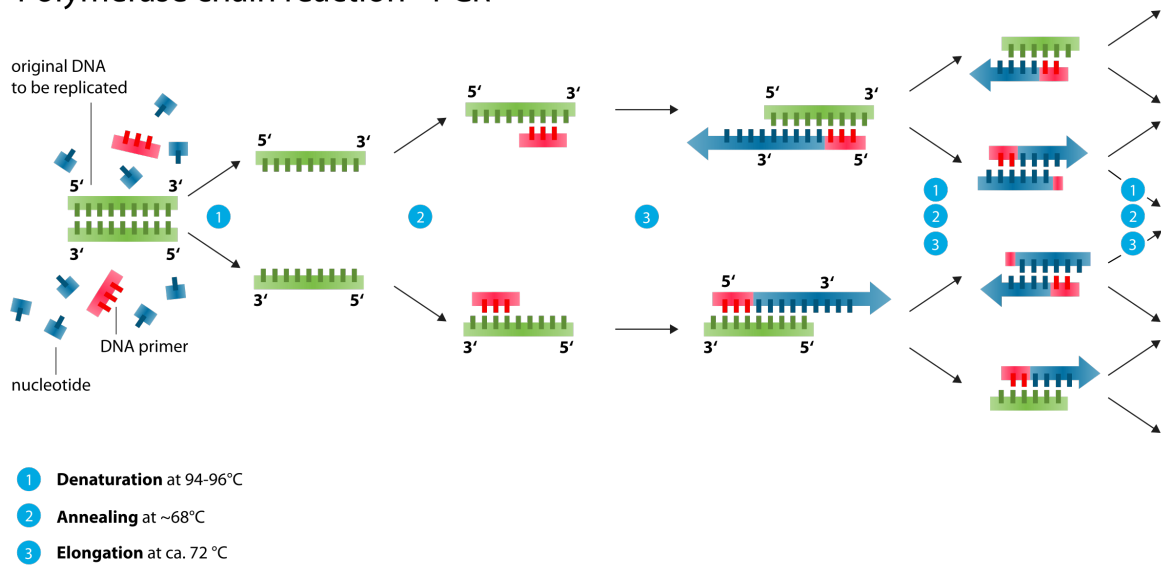


Fig. 1-1: Schematic diagram of polymerase chain reaction process [10].

Since PCR technology can rapidly and sensitively amplify the target gene, it can be used for the diagnosis of infectious diseases caused by pathogens. Since the PCR technique exponentially amplifies the target DNA sequence, the sensitivity of this technique is extremely high. Real-time based PCR can even detect samples containing only 5 pathogenic cells.

1.2.2 ELISA Assay

ELISA) assay is a kind of enzyme immunoassay technology which was first described by Weiland in 1978 [5]. In ELISA method the enzyme molecule is covalently bound to the antibody or the anti-antibody molecule, and such binding does not change the immunological properties of the antibody nor affect the biological activity of the enzyme. Such an enzyme-labeled antibody can specifically bind to an antigen or antibody adsorbed on a carrier. After the substrate solution is added drop by drop, the substrate can be converted into a colored oxidized form by a colorless

reduced form of the hydrogen donor contained by the enzyme, and a color reaction occurs. Therefore, the color reaction of the substrate can be used to determine whether or not there is a corresponding immune response. The depth of the color reaction is proportional to the amount of the corresponding antibody or antigen present in the sample [11]. Because ELISA is fast, sensitive, simple, and easy to standardize, it is widely used in the detection of a variety of bacteria and viruses.

1.3 Sensor Based Pathogen Detection Methods

Different from traditional bacterial detection methods, sensor based pathogen detection methods usually introduce a physical parameter to detect the pathogen by directly measuring the physical properties of bacteria or converting signals into electrical signals. Although the sensitivity of sensor based pathogen detection methods are typically less than the conventional methods, they are less expensive in experiment and shorter in detection time.

1.3.1 Impedance

Cells and its corresponding antibodies are specific to each other. Based on this principle, we can use different antibodies to capture the targeted cells from the mixed solution and immobile them on the circuit. Since the attachment of cells will change the impedance of the circuit, the number or concentration of target cells can be calculated very accurately by measuring the change in impedance [12, 13]. In order to get a precise result, impedance-based microfluidic detectors usually integrate a high-density electrode array on the surface of the microfluidic channel. The antibody is attached directly to the electrode and captures the target cells in the mixed solution flowing through the channel. In some cases, we can also use special immune-magnetic beads to

mark target cells in advance (Fig 1-2). Thus, cells can be immobilized on the electrodes by magnetic beads without using antibodies [12].

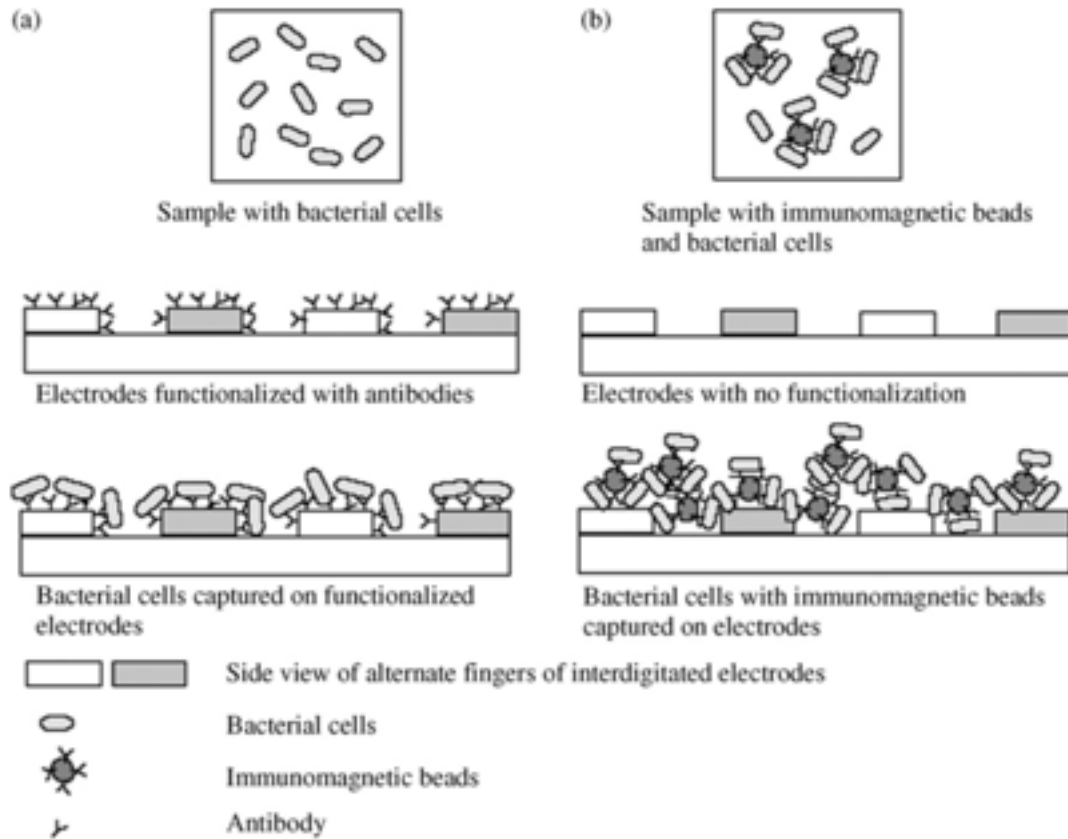


Fig. 1-2: Conceptual view of impedance-based microfluidic detectors. (a) The antibody is immobilized on the electrode in advance to capture the passing target cells. (b) The electrode array does not do any treatment. The target cells are labeled with immune-magnetic beads in advance. When the labeled cells flow through the electrode array, the immune-magnetic beads are attracted by the electrodes and adsorbed on the it together with the cells [12].

Compared with directly immobilizing the antibody on the electrode array, the advantages of using immune-magnetic beads labeling is that the cell capture rate is high, and since the electrode array

is not subjected to pretreatment, which will make the operation difficulty lower and improve the chip reuse rate.

1.3.2 Microfluidic Activated Pathogen Detection

Microfluidic is a technology that aims to precisely control, manipulate, and detect small amount of complex fluid at microscopic dimensions. It focuses on building microfluidic channel systems to perform a variety of complex microfluidic manipulation functions. Microfluidic technique was invented in early 1980s. Similar to regular fluidic systems, the devices required for microfluidic systems also include pumps, valves, mixers, filters and separators. Since microfluidic devices typically have dimensions controlled at the micron and sub-micron level, they can greatly attenuate the effects of gravity from the earth. However, on the other hand, the surface-to-volume ratio of small-scale channels will become very large, which causes the surface tension, capillary forces and the fluid viscous forces and often these forces start to dominate in the system [14,15]. Due to its great potential applications in the field of biology, chemistry and medicine, microfluidics has been developed as a new interdisciplinary research field involving biology, chemistry, medicine, fluids mechanics, electronics, material science, and other disciplines.

1.4 Outline of this Thesis

According to the record from Centers for Disease Control and Prevention. *Salmonella* infection has not declined in 15 years [16]. One of the important reason is *Salmonella* can be carried by many different types of foods like meats, fruits, vegetables and even processed foods. Therefore, the separation chip for *Salmonella* must have good universality and can accurately detach the *salmonella* out from different complex environment. Most of the current pathogen separation chips

are not satisfactory in dealing with complex bacterial mixed solutions, usually they need to know all the components in the solution and test each one's inverse frequency [17-19].

As part of this work, we aim to design an Alternative Current-DEP Field flow fractionation (DEP FFF) type micro fluidic chip which will detach the *S. typhimurium* from complex mixed culture solution with high efficiency. By using MatLab, we first indicate how Clausius-Mossotti (CM) factor acts respect to the permittivity and the conductivity of the particle and the medium. After that, we designed the device by using COMSOL Multiphysics and analyze the influence of various factors on the separation rate.

CHAPTER II

LITERATURE REVIEW

2.1 Microfluidic Lab-on-a-chip

Microfluidic lab-on-a-chip is a kind of novel technology which aims to integrate the entire laboratory functions including sampling, dilution, reagent addition, reaction, separation and detection on the micro size chip. Because in the micron-scale channels, the fluid will exhibit a special performance that is different from the macroscopic scale. Therefore, the microfluidic chip has the characteristics of controllable liquid flow, minimal consumption of samples, and high analysis efficiency [20]. Due to its unique advantages of precision in detection, fast response time and low cost associated with it, microfluidic lab-on-a-chip has been widely used for rapid detection and separation of various bio-micro-molecules.

2.2 Dielectrophoresis

Dielectrophoresis (DEP) is a kind of force and it arises when a dielectric particle passing through a non-uniform electric field. The subject particle does not require to be charged. DEP will happen in both DC electric field and AC electric field. An inhomogeneous electric field will polarize the particles by shifting the charges inside the particle. The force acting on the either side of the polarized particle will be different and this will generate a net force and move the particle. This phenomenon was first discovered in early 20th century and reported by Herbert Pohl in the 1950s [21].

The magnitude of the DEP force is mainly determined by the frequency and magnitude of the externally applied electric field, the electrical properties of the particles and solution, and the shape and size of the particles. When the electrical polarizability of the particles is larger than the surrounding medium, the direction of the DEP force will point to the increasing electric field strength regions and called positive dielectrophoresis (pDEP). In contrast, if the electrical polarizability of the suspending particles is less than the surrounding medium, the direction of the DEP force will point to the decreasing electric field strength regions and called negative dielectrophoresis (nDEP). Since the relative polarizabilities of the suspending particles and surrounding medium are frequency-dependent, it let us possible to change the direction of the DEP force by manipulate the frequency of the electric field.

2.2.1 Single Membrane Spheres Particles

Let us assume that the suspended cells are spherical particles with a single layer membrane shown in Fig.2-1. Let us also assume that the sphere particle has a radius r , absolute permittivity ϵ_p and suspended in a dielectric fluidic medium of absolute permittivity ϵ_m . When the mixed solution passes through a direct current (DC) electric field of strength E , the time-averaged DEP force acting on the particle is given by [22,23,25].

$$F_{DEP} = 2\pi\epsilon_m r^3 Re(K_{CM}) \nabla |E_{RMS}|^2 \quad (2.1)$$

In (2.1), E is the strength of the applied direct current inhomogeneous electric field, K_{CM} is the Clausius-Mossoti factor [25]. K_{CM} , can be expressed by equation (2.2):

$$K_{CM} = \frac{\epsilon_p - \epsilon_m}{\epsilon_p + 2\epsilon_m} \quad (2.2)$$

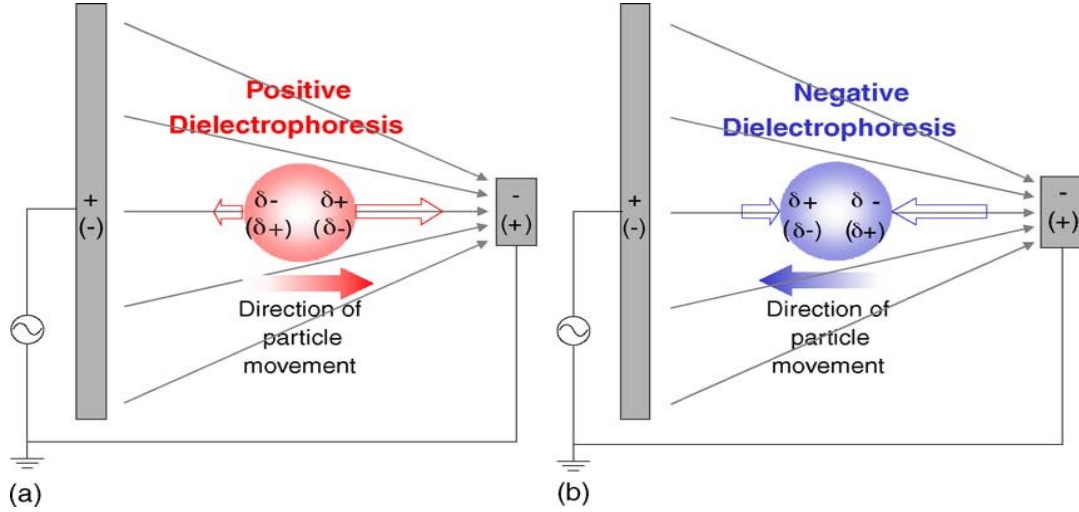


Fig. 2-1: Schematic diagram of non-uniform electric field and induced particle. The electrode on the right side has less area and will produce a stronger electric field than the left side. (a) Particles with a higher polarizability than the surrounded medium will receive positive DEP force and move to the right side. (b) Particles with a lower polarizability than the surrounding medium will receive positive DEP force and move to the left side [24].

From equation (2.2), we can easily find that when the absolute permittivity ϵ_p of the suspending particle is larger than the absolute permittivity ϵ_m of the surrounding medium, the value of K_{CM} will be positive, F_{DEP} will become positive and will push the particle towards the high electric field region. On the other hand, if the absolute permittivity ϵ_p of the suspending particle is lower than the absolute permittivity of the surrounding medium, ϵ_m , the value of K_{CM} will be negative. For this case, the value of F_{DEP} will become negative and will push the particle away from the high electric field region.

2.2.2 Single Membrane Ellipsoids Particle

In practical applications, the shape of the cells usually appears elliptical rather than a sphere. Therefore, the stress of the cells in the non-uniform electric field and the expression of the DEP force will be different from what is expressed in equation (2.1). Let us assume an ellipsoid particle with shape and dimensions mentioned in Figure 2.2. The principle and semi-axis of this ellipsoid have the dimensions of a, b and c as shown in Figure 2.2. When we apply a DC electric field with intensity E along the x-axis the.

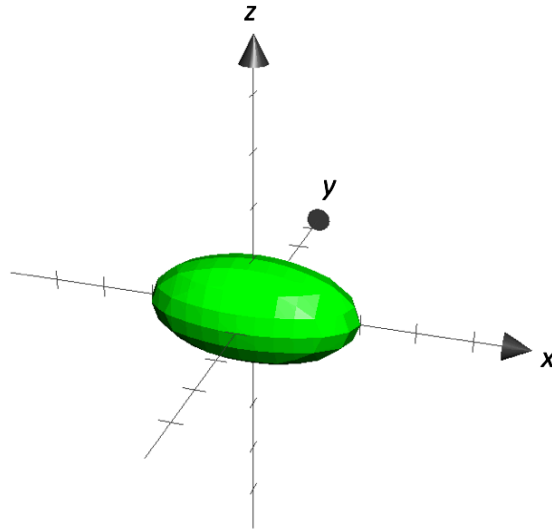


Fig. 2-2: Schematic diagram of an ellipsoids particle with principle semi-axis of a, b and c along axis x, y and z respectively.

time-averaged DEP force act on the particle can be expressed by the equation (2.3) [25]:

$$F_{DEP} = \frac{2\pi abc}{3} \epsilon_m \text{Re}(K_{CM}) \nabla |\vec{E}|^2 \quad (2.3)$$

Where

$$K_{CM} = \frac{\epsilon_p - \epsilon_m}{\epsilon_m} \quad (2.4)$$

2.2.3 Alternative Current-Dielectrophoresis

In the real system, the dielectric permittivity for both suspending particles and surrounding medium are complex in nature and has both real and imaginary parts as mentioned by equation

$$(2.5). \quad \varepsilon^* = \varepsilon - j \frac{\sigma}{\omega} \quad (2.5)$$

where ε^* is the dielectric permittivity of the material, ε is the dielectric constant, σ is the electrical conductivity, j represents imaginary vector ($j^2 = -1$) and ω is the frequency of the applied electric field [26]. In the case of direct current-DEP, the frequency is zero we have $\varepsilon_p^* = \varepsilon_p$ and $\varepsilon_m^* = \varepsilon_m$. In the case of alternative current-DEP, the imaginary part will be in effect. For single membrane sphere particles, the expression of the time-averaged DEP force becomes:

$$F_{DEP} = 2\pi\varepsilon_m r^3 \text{Re}(K_{CM}) \nabla |E_{RMS}|^2 \quad (2.6)$$

where

$$K_{CM} = \frac{\varepsilon_p^* - \varepsilon_m^*}{\varepsilon_p^* + 2\varepsilon_m^*} \quad (2.7)$$

For single membrane Ellipsoids particles, the expression of the time-averaged DEP force becomes:

$$F_{DEP} = \frac{2\pi abc}{3} \varepsilon_m \text{Re}(K_{CM}) \nabla |\vec{E}|^2 \quad (2.8)$$

where

$$K_{CM} = \frac{\varepsilon_p^* - \varepsilon_m^*}{\varepsilon_m^*} \quad (2.9)$$

Since the CM factor is the only parameter that determines the direction of the DEP force, therefore, the use of an alternating electric field makes it possible to change the direction of the DEP force under certain circumstances.

2.3 Dielectrophoresis Based Microfluidic Chip

Usually cells are also dielectric particles and hence, they are polarized and subject to DEP forces when passing through a non-uniform electric field (Fig. 2-3). The magnitude and direction of the DEP force is highly dependent on the electrical properties of the suspending cells and the surrounding medium [22,23,27]. Compared to impedance-based microfluidic chips, DEP-based chips do not require tedious pre-treatment of cells or chips prior to experimentation, thus greatly reduces the cost and improves the efficiency of detection process. Therefore, the detection and separation of cells by DEP had been used extensively for various applications [18].

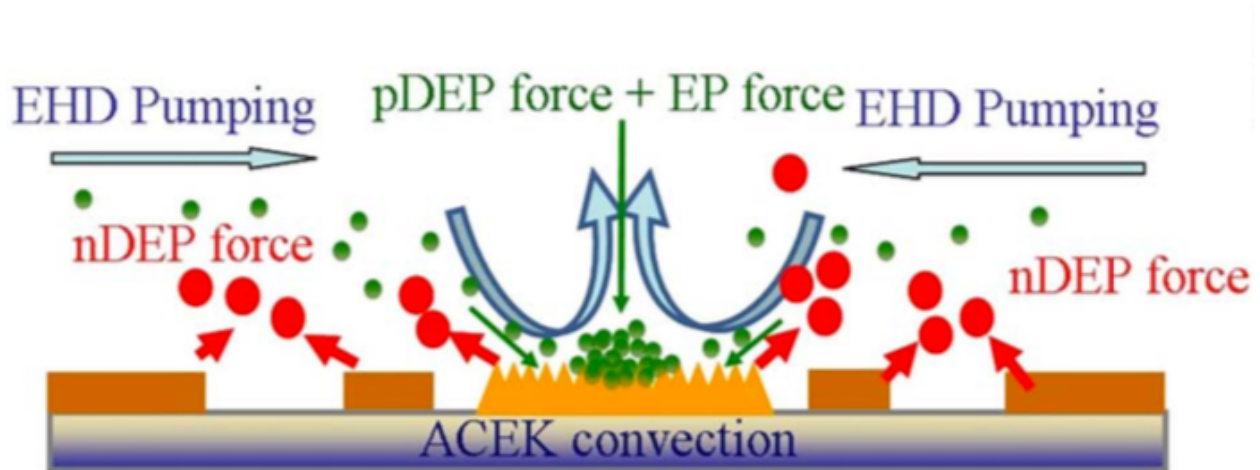


Fig. 2-3: Schematic illustration of the DEP force acted on the dielectric particles [28].

In the past several decades, various methods had been proposed to separate food borne pathogens by using DEP based microfluidic chip. DEP based microfluidic chips are generally divided into several categories which are mentioned in the following subsections.

2.3.1 Non-field flow fractionation(FFF)

Non-field flow fractionation (FFF) is a conventional way to separate particles via AC-DEP. By driving appropriate frequencies, different types of bacteria are subjected to DEP forces with different magnitude and directions, which will lead them to separate from each other (Fig. 2-4). In 1996, Pethig et al designed a chip with an interdigitated, castellated microelectrode to detect yeast [29].

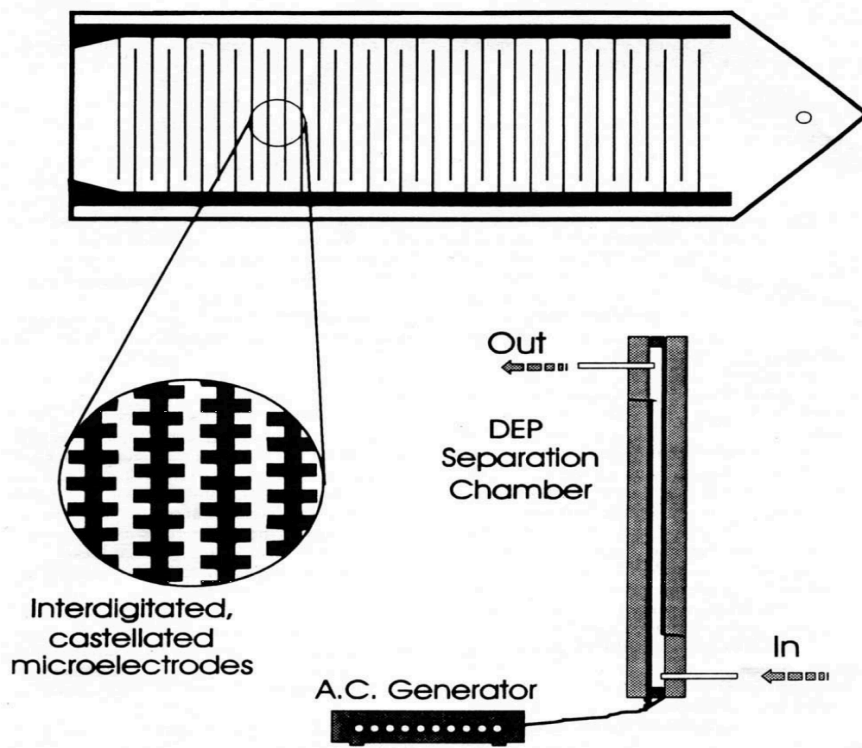


Fig. 2-4: Design for a DEP separation chamber consist of inlet channel, outlet channel, AC current generator and interdigitated castellated microelectrodes [29].

The shape of the entire device is a simple rectangular parallelepiped with the electrode array generated inside. The cell mixture- viable and nonviable yeast-is injected into the chamber via inlet channel until the entire separation chamber is filled. After that, an AC current is supplied to the electrode array with appropriate magnitude and frequency, to maximize both the positive and

negative DEP forces. After sometime the viable yeast cells are collected by the positive DEP force and attached on the edge of the electrode array while the nonviable cells were dragged under negative DEP force and aggregated to form a triangular shape in the regions with low electric field strength (Fig. 2-5).

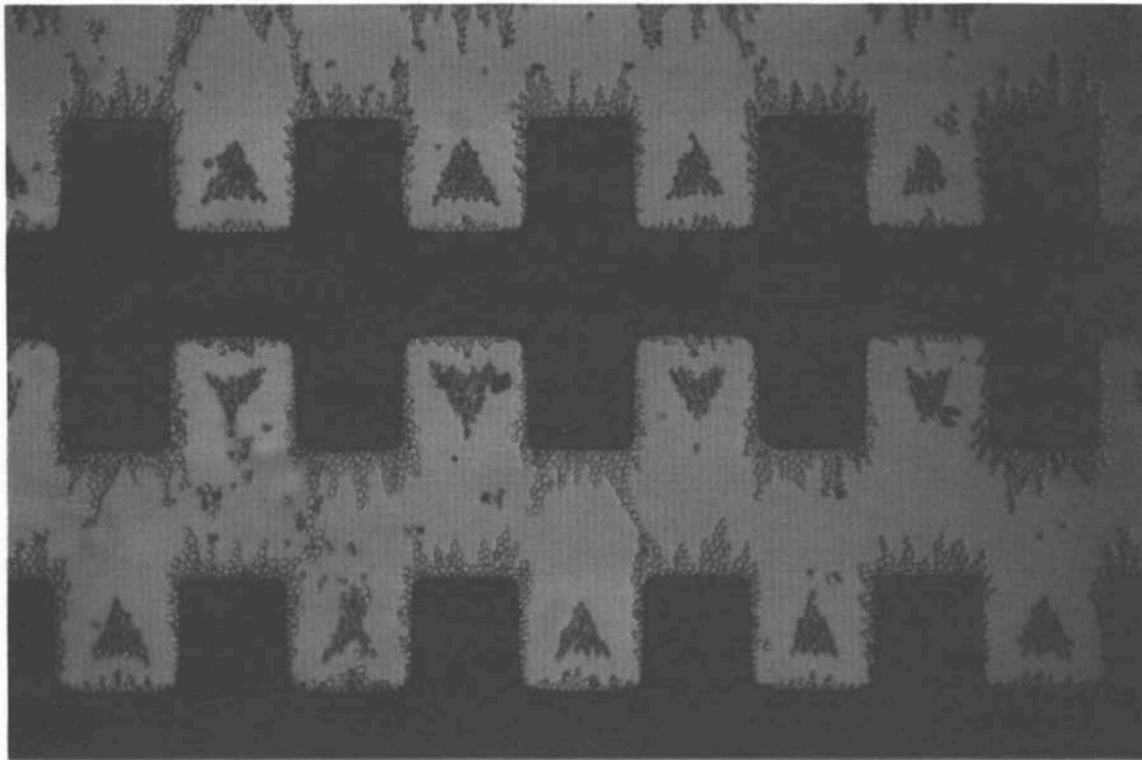


Fig. 2-5: The separation of mixed viable and nonviable cells. The viable cells dragged by positive DEP force and stick on electrode array, while the nonviable dragged by negative DEP force and move away from the electrode array [29].

After the separation process is done, the nonviable cells are taken out by using the fluidic pump. Then, the frequency of the electric field is varied to make the negative DEP force and take out the viable cell out from the electrode array. Although this method successfully isolated the viable and nonviable yeast cells, it has some disadvantages as well. This process is slow as it takes sometime to completely attach the targeted cells on the electrode. Also, since a single outlet is shared, a

considerable portion of nonviable cells remained in the channel and mixed with the viable cells and reduces the separation rate.

2.3.2 Field flow fractionation (FFF)

Field flow fractionation (FFF) is a separation technique suitable for macromolecules, colloids, and micro particles. The basic principle of the technique is to apply a field in a direction perpendicular to the channel as the mixed solution flows through the flat microfluidic channel [30]. This way the particles in the solution are simultaneously subjected to channel flow and cross flow effect. Under the force exerted by the vertical field, particles will be separated and distributed on the different position across the channel due their distinct properties. Compared to the conventional Non-FFF model, FFF method is easier to operate and costs lower. The biggest difference between the two methods is that the FFF method involves with continuous micro-fluidic flow which will drag the separated cells through the channel and lead them go out from different outlet. Young-Ho Cho et al designed a chip with electrodes placed in the bottom of the channel [23]. This chip consists of three inlet channels, three outlet channels and one separation chamber (Fig. 2-6). The cell mixture (viable and nonviable yeast) was injected into the chip from inlet 1 located at the center of the chip. While the mixed solution passes through the separation chamber, the viable yeast will be subjected to negative DEP force and will move to the center of the channel. At the same time, the nonviable yeast will be subjected to the positive DEP force and move towards the side of the channel.

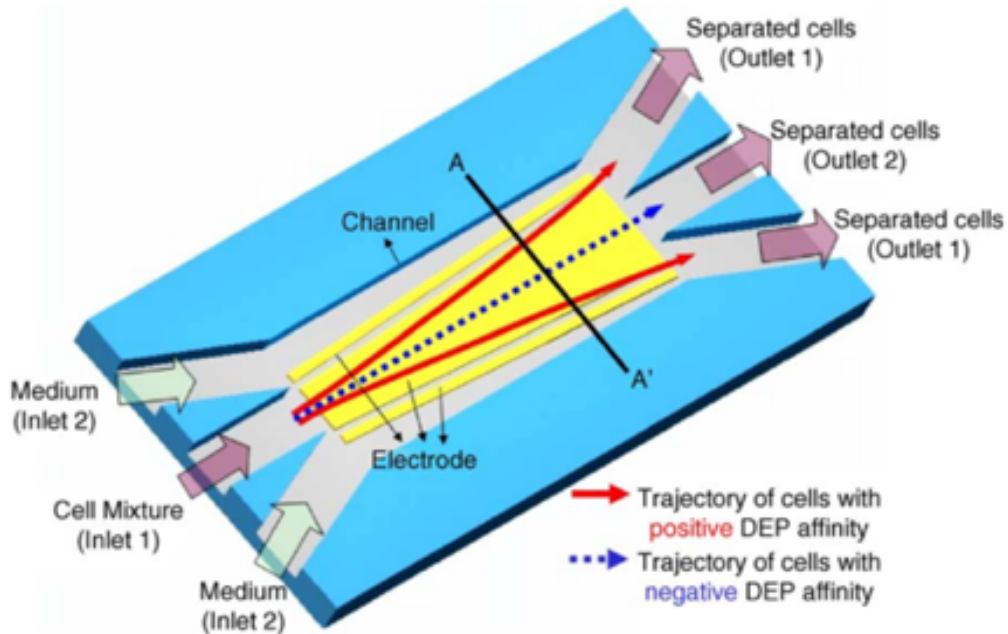
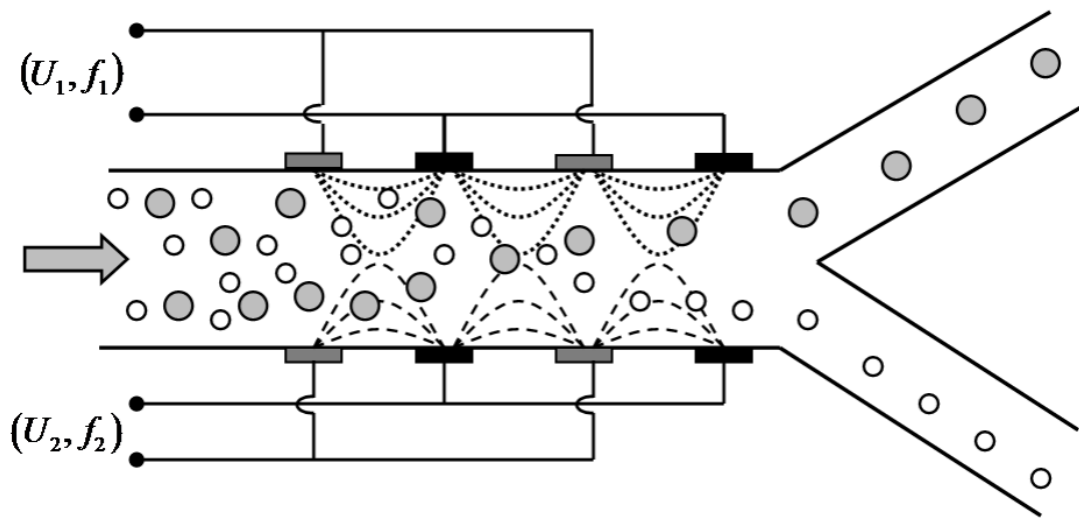


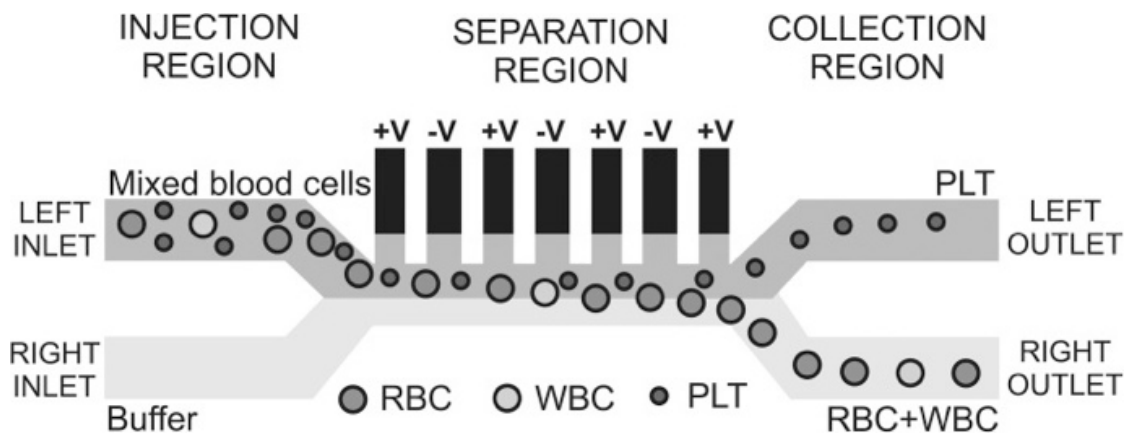
Fig.2-6: Schematic of a continuous cell separation chip using hydrodynamic DEP [23].

After the separation process, separation rates were found to be—around 97% for viable yeast cells and 64.5-74.3% for nonviable yeast cells, respectively. Due to the viscosity of the liquid, the flow rate of the liquid near the channel wall is much lower than the flow rate in the center of the channel. This leads to the fact that cells which were pulled towards the side of the channel by DEP force are prone to stagnate on the side wall of the channel. Therefore, the separation rate for nonviable yeast are lower than the viable yeast.

Based on the same concept, by arranging the electrode arrays with different shape or layout, a variety of chips are designed to handle different situations [31,32].



(a)



(b)

Fig. 2-7: (a) Schematic views of microfluidic chip with electrodes array generated on both of the side wall [31]. (b) Schematic of the chip design, electrodes array was placed on one of the side wall [30].

Fig. 2-7 shows two different types of FFF separation chip with the electrode arrays were placed on the side of the fluidic channel [30,31]. By fabricating the electrode arrays separately on the opposite sides of the wall will help us to maximum the DEP force acting on the particles.

2.3.3 Gravity involved FFF

In order to get higher separation efficiency, some groups bring in some other forces to assist the separation process. One of the classic designs was involving the gravity force (Fig. 2-8).

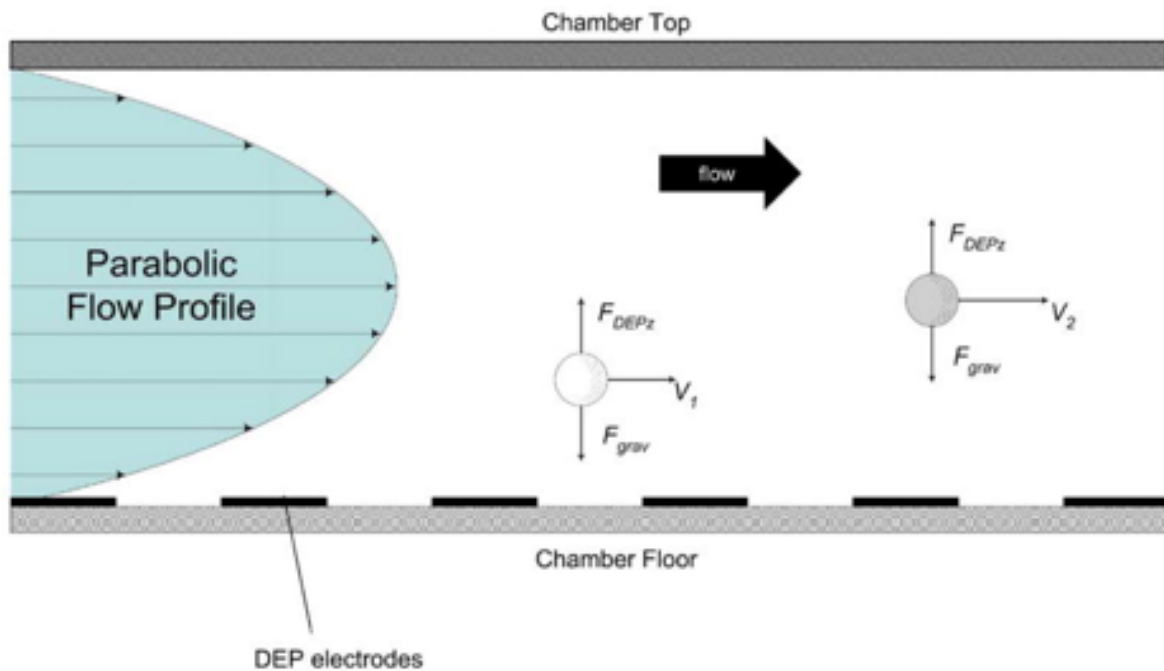


Fig. 2-8: Side view of the chamber and the force diagram of the particle [33].

Inside the fluidic chamber, the DEP force will be decreased when it is away from the electrodes array. So, different cells with different density will be balanced at different levitation heights. Due to the hydrodynamic flow profile, the flow speeds at different heights are not equal which allow us to collect different groups of cells at different time.

2.3.4 DC-DEP FFF

By setting some isolated barriers inside the microfluidic channel, some groups design a static non-uniformly distributed E-field inside the channel. This kind of design does not need to apply alternative current and can rapidly finish the separation. The separation process will not only rely on the electrical properties of the particle but also highly dependent on the size of the particle (Fig. 2-9).

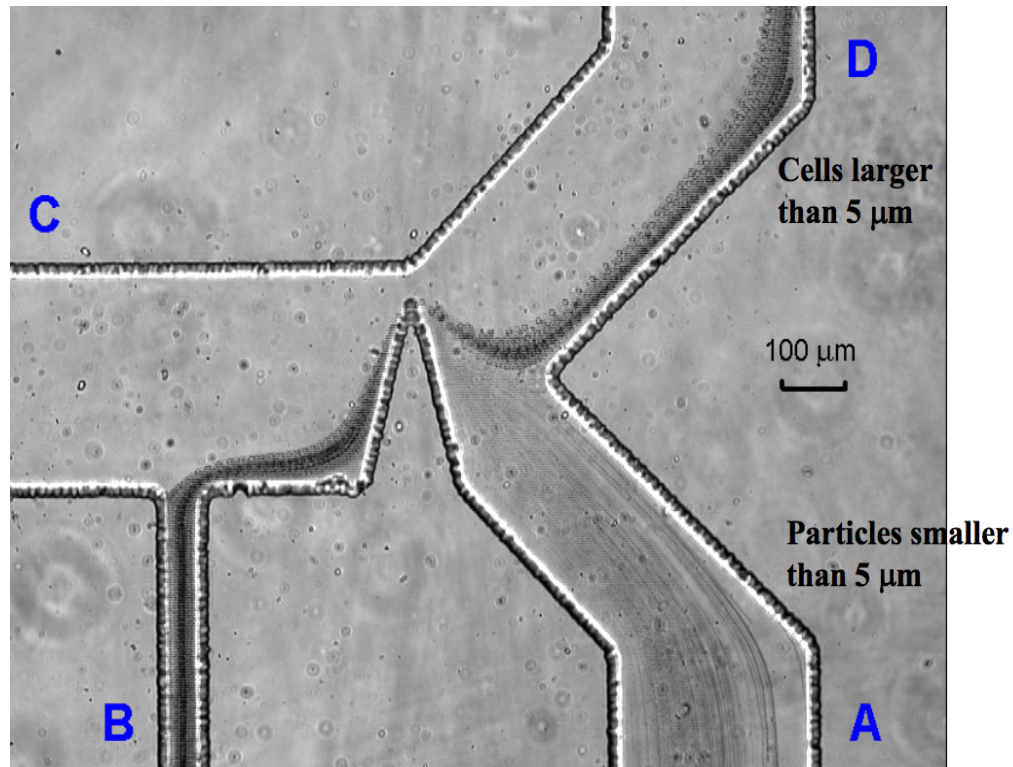


Fig. 2-9: DC-DEP particle separation chip using triangular hurdle with divergent output branches [34].

Kang et al designed a type of DC-DEP separation chip with a triangular hurdle placed inside the channel. When mixed solution crosses over the hurdle, in addition to the DEP force particles will be subjected to centripetal force. Under the combined effect of the two, large-sized cells will be pulled upwards and flow out from the D outlet, while small-sized particles will be pulled downwards and will flow out from the A outlet.

CHAPTER III

MATERIALS AND METHODS

3.1 Electrical Properties of Pathogens

It was discussed in chapter II that the bacteria cell can act like a dielectric particle. Fig. 3-1 illustrates the structure and contents of a typical bacteria cell. Since the cytoplasm of pathogen contains a large number of ions, it can make the dielectric effect of the bacteria much stronger. Also, Ferrer et al. [35] found that the living environment will greatly affect the cell's dielectric constant because living cells will continuously exchange substances with the outside world.

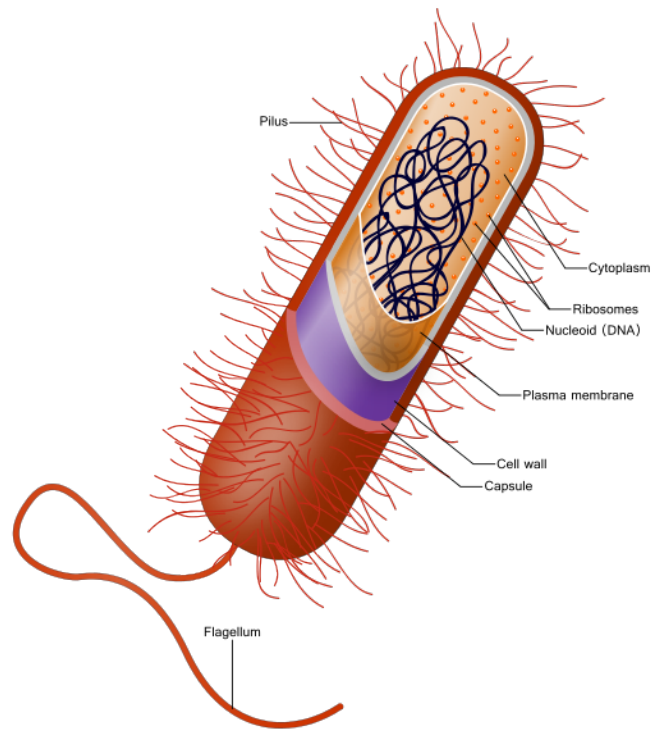


Fig. 3-1: Schematic diagram of a bacteria [36].

Based on that, we first used MatLab to theoretically explained how CM factor acts with respect to the electrical properties of the suspending pathogen and the surrounding medium.

3.2 Design and Simulation of the Microfluidic Chip

We used the finite analysis software COMSOL to design the microfluidic chip and simulate the separation process. COMSOL Multiphysics is a cross-platform finite element analysis solver and Multiphysics simulation software which is widely used in scientific research, engineering calculations and simulating various physical processes. Based on the finite element method, COMSOL Multiphysics simulates real-physical phenomena by solving partial differential equations under various boundary conditions.

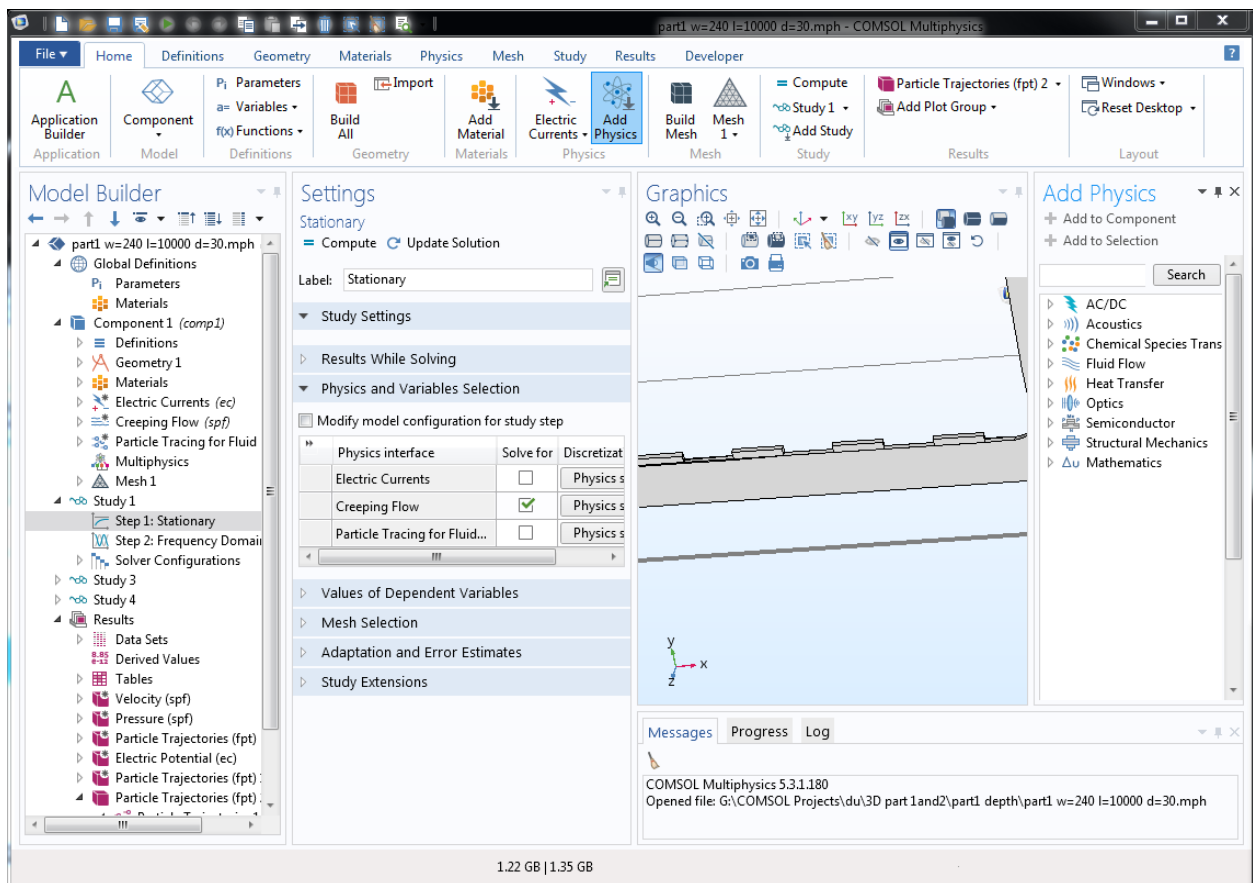


Fig. 3-2: Operation window for COMSOL Multiphysics.

In our case, we first used the 3D model builder to build the geometry structure of our microfluidic channel. After that we added the electric current module, creeping flow module and particle

tracking module to simulate the pathogen separation process. Finally, we applied the stationary study to creeping flow process, the frequency domain study to electric current and the time dependent study to the particle tracking simulation. Fig. 3-2 shows the operation window for COMSOL Multiphysics software.

3.2.1 Parameters and Constant Values

In the global definition section, we defined various parameters we used and the variables we applied in the simulation process. The value and definitions are mentioned in table 3-1.

Table 3-1: Parameters and variables used in simulation

<i>Name</i>	<i>Expression</i>	<i>Description</i>
f0	450 [kHz]	Frequency of the electric field
sigma_f	55[mS/m]	Fluid medium conductivity
epsilon_f	80	Fluid relative permittivity
rho_f	1000[kg/m ³]	Fluid density
mu_f	1e-3[Pa*s]	Fluid dynamic viscosity
rho_p	1050[kg/m ³]	Particle density
dp1	2[um]	Particle diameter: Particle 1
dp2	3[um]	Particle diameter: Particle 2
dp3	4[um]	Particle diameter: Particle 2
sigma_p1	0.31[S/m]	Particle conductivity: Particle 1
sigma_p2	0.31[S/m]	Particle conductivity: Particle 2

sigma_p3	0.31[S/m]	Particle conductivity: Particle 3
epsilon_p1	7	Particle relative permittivity: Particle 1
epsilon_p2	19	Particle relative permittivity: Particle 2
epsilon_p3	24	Particle relative permittivity: Particle 3
sigma_s1	5e-6[S/m]	Shell electrical conductivity: particle 1
sigma_s2	5e-6[S/m]	Shell electrical conductivity: particle 2
sigma_s3	5e-6[S/m]	Shell electrical conductivity: particle 3
epsilon_p1	10	Shell relative permittivity: Particle 1
epsilon_p2	80	Shell relative permittivity: Particle 2
epsilon_p3	80	Shell relative permittivity: Particle 3
th_s1	25[nm]	Shell thickness: Particle 1
th_s2	65[nm]	Shell thickness: Particle 2
th_s3	65[nm]	Shell thickness: Particle 3
V0	50[V]	Applied voltage

3.2.2 Geometry Build

In addition to importing CAD geometry from external third-party platforms, COMSOL Multiphysics itself contains a certain number of built-in modeling tools that allow users to model directly in the software.

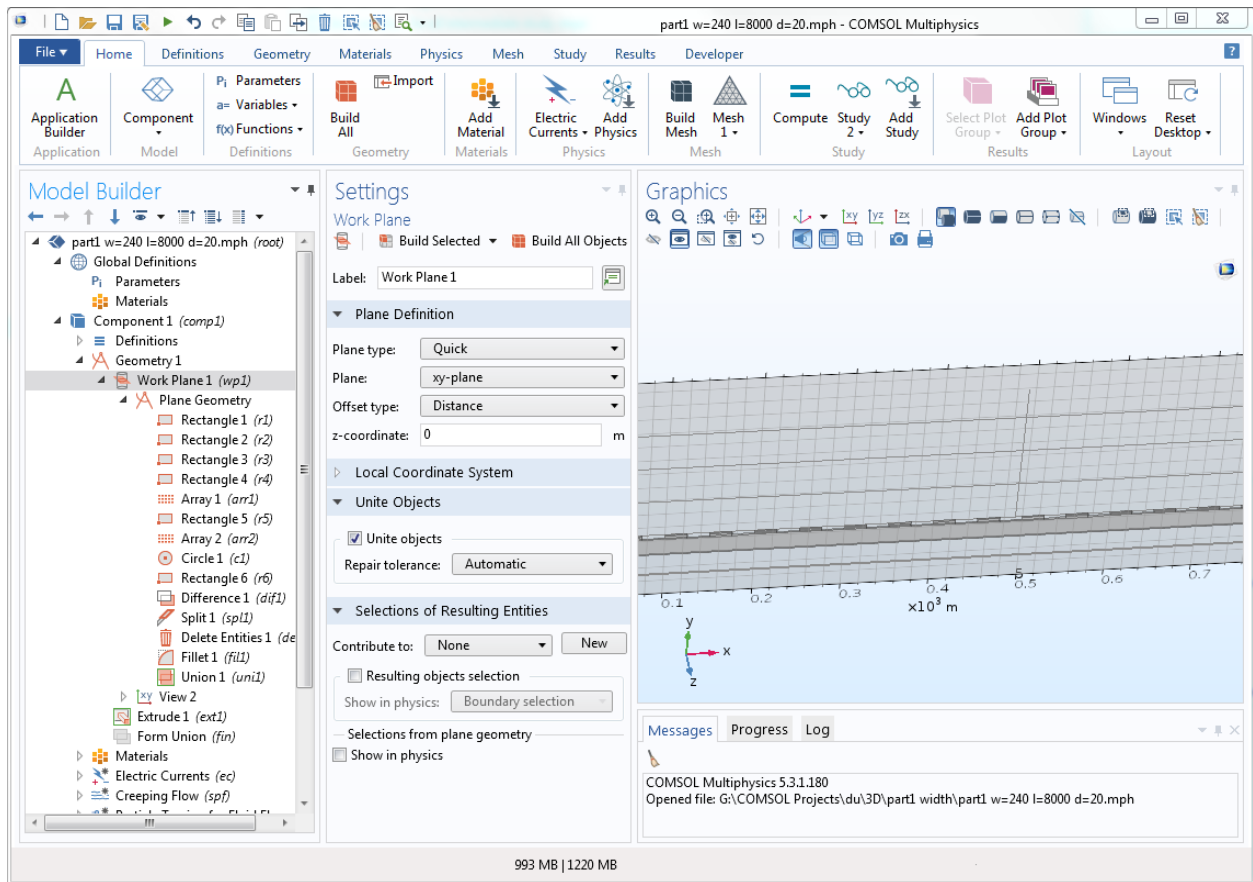


Fig. 3-3: Geometric modeling window of COMSOL Multiphysics

COMSOL Multiphysics provides several model components for users. For different application requirement, user can directly build their geometry under zero dimension (Point), one dimension (line), one dimension axisymmetric, two dimension (Plane), two dimension axisymmetric and three dimension. In some special cases, we can also build some symmetric 3D geometry via sweep or extrude the 2D geometry. Fig. 3-3 shows the process by which we build our model. We first completed the construction of the 2D model on the work plane. The channel was built in rectangle shape and electrode arrays were placed on the right side of the main channel with a certain ratio separate from each other. After building the 2D structure, we extruded the 2D geometry to a certain distance to form the 3D channel. The distance we extruded was the depth of the channel.

3.2.3 Addition of Physics Module

COMSOL Multiphysics currently have one basic module and eight professional modules: Structural Mechanics Module, Chemical Engineering Module, Heat Transfer Module, Earth Science Module, RF Module, AC/DC Module, MEMS Module, Acoustics Module. There are many sub-modules under each large module for more accurate simulation.

In our case, the simulation of the bacterial separation process consists of three physical modules: Electric Current, Creeping Flow and Particle Tracing for Fluid Flow.

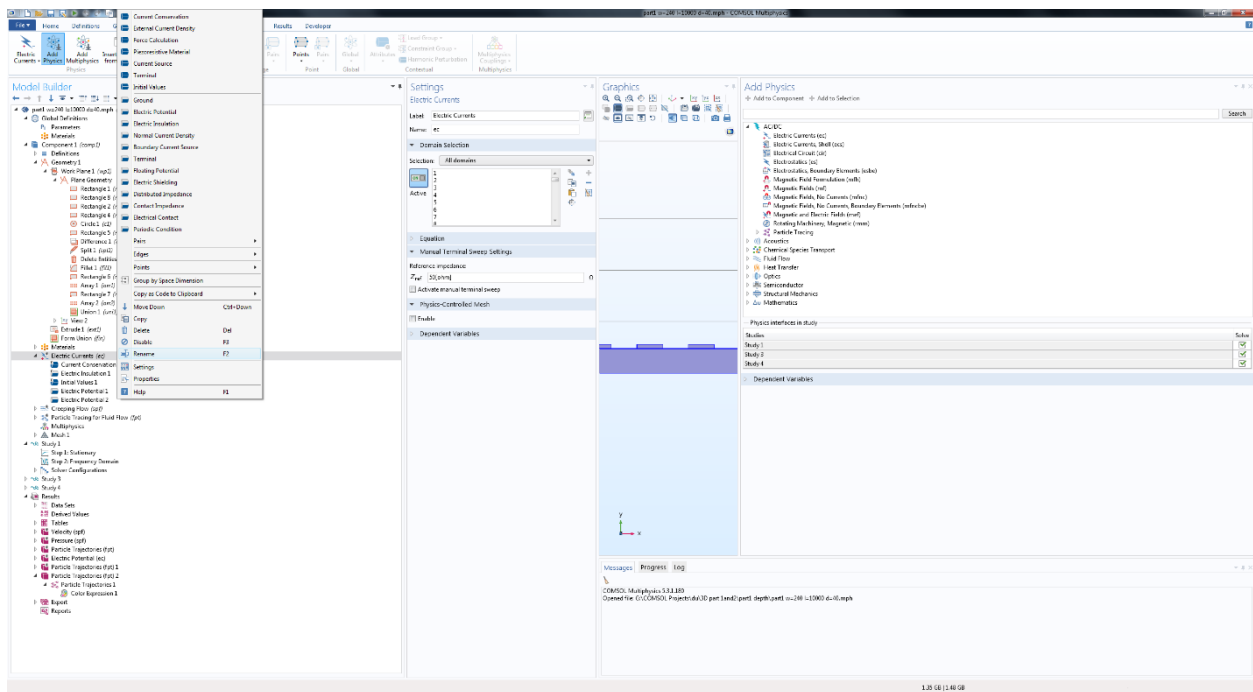


Fig. 3-4: AD/DC physics module and its component.

The AC/DC module allowed us to create an electric field by adding charge, current and voltage to the model. In our case, the AC/DC module was used to apply the voltage through the electrode.

By applying the voltage to the electrode arrays, we can create a non-uniform electric field inside the separation chamber. In our model, we applied five components: Current conservation, Electric insulation for boundary condition, initial values, electric potential 1 to the positive electrode array and electric potential 2 to the negative electric array.

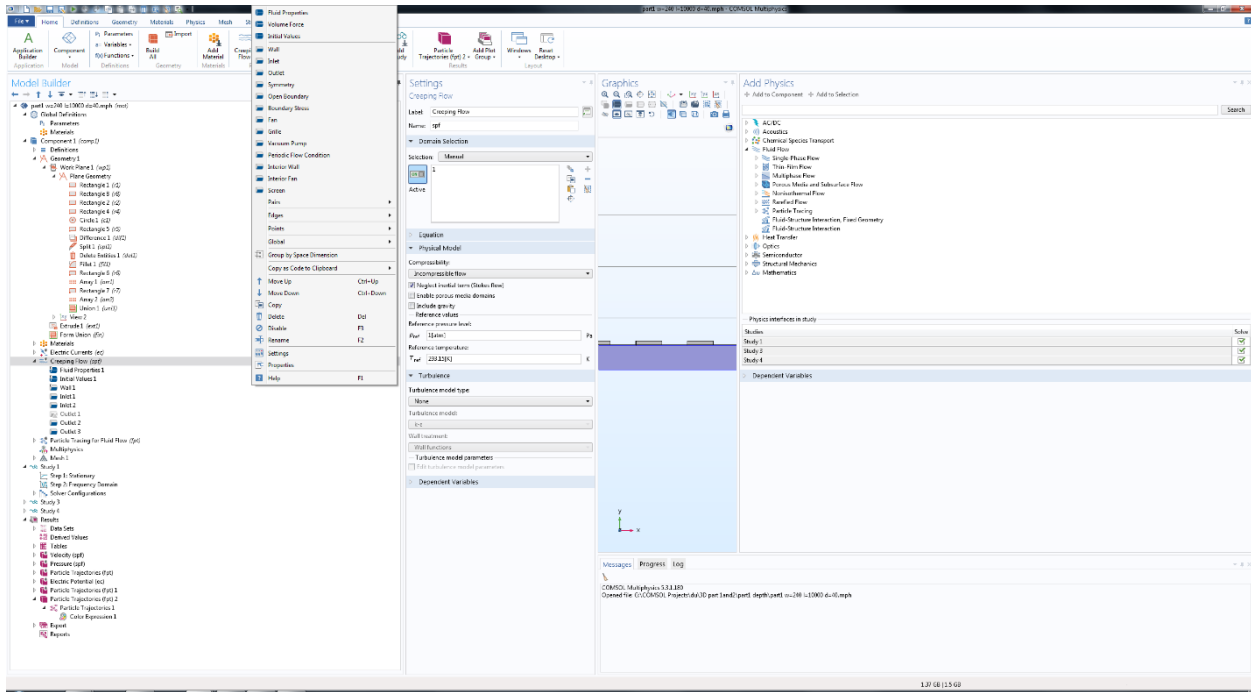


Fig. 3-5: Creeping flow physics module and its component

The COMSOL Multiphysics offers a variety of fluid flow modules to handle different situations. We have adopted the simplest single-phase creeping flow, since our microfluidic channels are using straight line structures (Fig. 3-5).

In this module, the users can specify the inlet and outlet of the channel, the parameters such as the density and viscosity of the liquid, the initial velocity profile of the fluid and the boundary

conditions. We added nine components in this module: fluid properties, initial values, boundry wall, three inlets and three outlets.

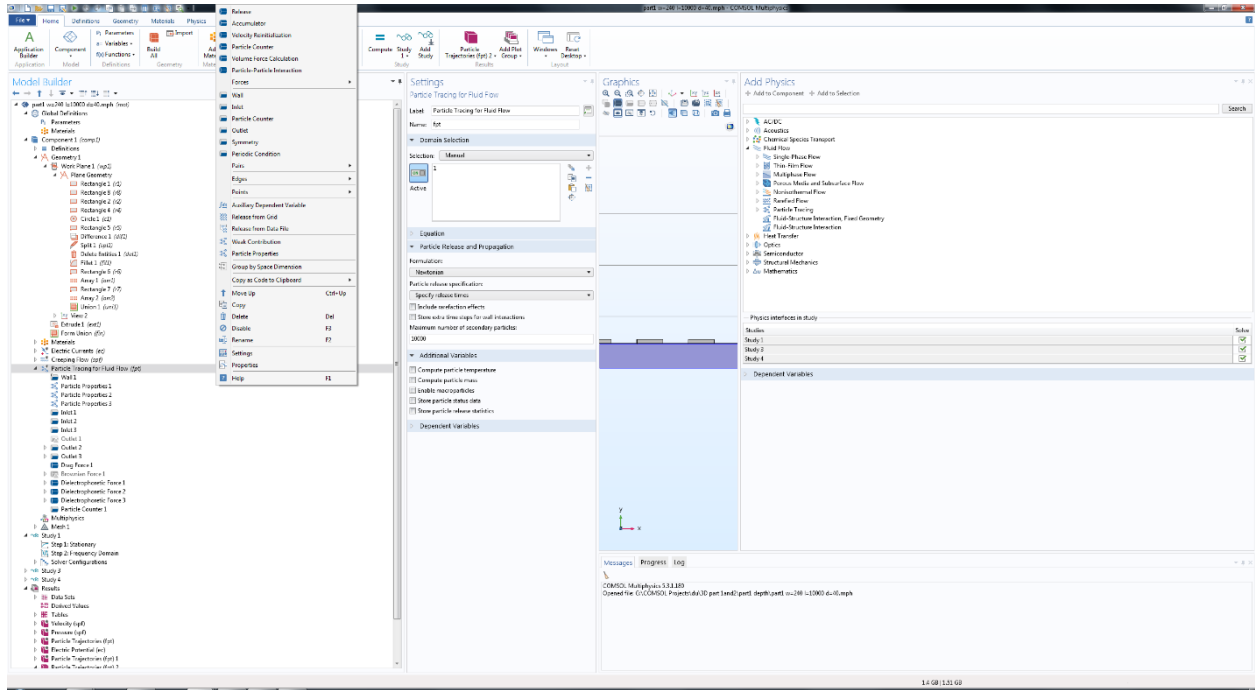


Fig. 3-6: Particle tracking for fluid flow

Under the fluid flow module, the users can find the particle tracking module specific for tracking the uncharged particles (Fig. 3-6). This module allows users to define multiple particles with their distinct properties and applying several forces subject to the particle. In our case, we defined three different particles with different electrical properties. We also applied drag force and dielectrophoretic force subject to the particles which generated by the fluid flow and non-uniform electric field, respectively. Finally, we added the particle counter at each outlet to collect the data.

3.2.4 Study

According to different physical processes, COMSOL Multiphysics provides several calculations include continuous, discrete, stationary and time dependent study.

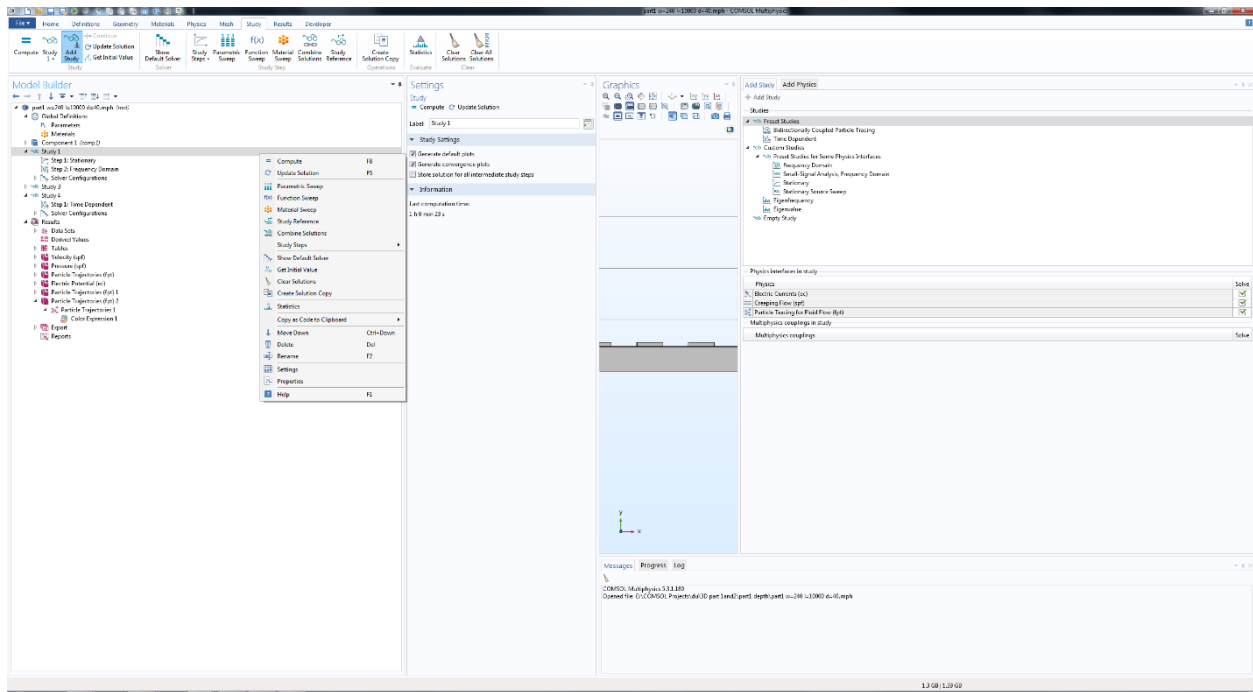


Fig. 3-7: Study options for COMSOL Multiphysics.

In our study, we simulated the separation in two steps. The first step, we solved the creeping flow and electric current under stationary and frequency domain study, respectively. In the second step, we solved the particle tracing under time dependent study. In the graphic window of Fig. 3-7, we can monitor the separation process to view how the particle been isolated from each other and flow out through different outlet.

CHAPTER IV

RESULTS

4.1 Clausius-Mossotti Factor

Based on the theoretical concept described in chapter II, we can conclude that only the K_{CM} factor will determine the direction of the DEP force. Assuming that all bacteria are of spherical in shape, the expression of the Clausius-Mossotti (CM) Factor can be simplified to

$$K_{CM} = \frac{\varepsilon_p^* - \varepsilon_m^*}{\varepsilon_p^* + \varepsilon_m^*} \quad (4.1)$$

Where

$$\varepsilon_p^* = \varepsilon_p - j \frac{\sigma_p}{\omega} \quad (4.2)$$

and

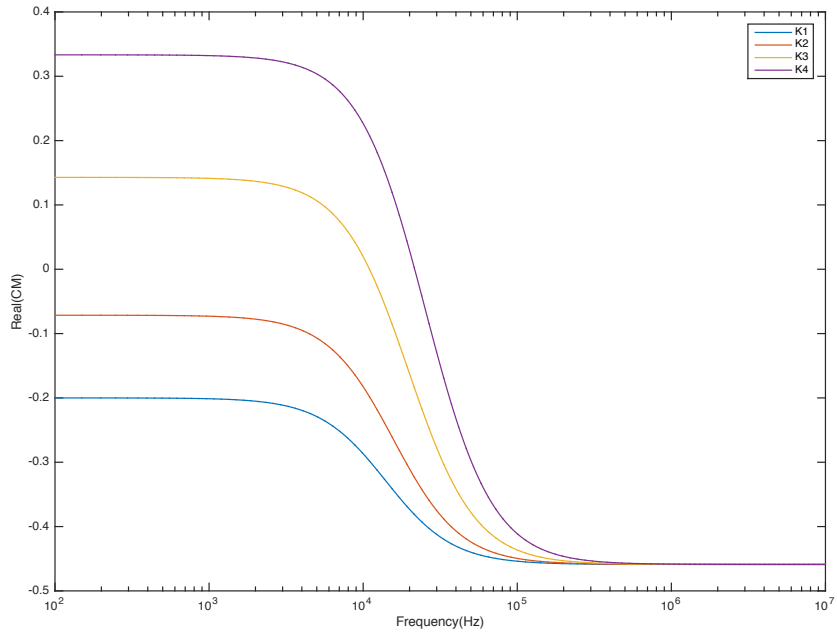
$$\varepsilon_m^* = \varepsilon_m - j \frac{\sigma_m}{\omega} \quad (4.3)$$

The relative permittivity and conductivity of the surrounding medium were set at 10 and 55 mS/m, respectively. We used four different particles with same conductivity 0.31 mS/m and the dielectric constant of these four bacteria are indicated in the table below,

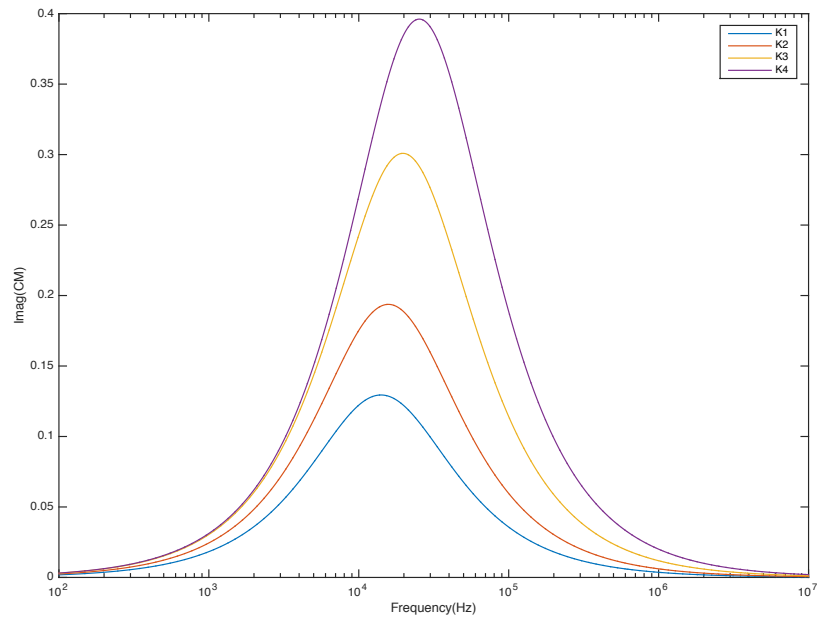
Table 4-1: Measured dielectric constant for four different bacteria under ambient and dry conditions [35].

BACTERICA	GRAM TYPE	$\epsilon_{r,eff,amb}$	$\epsilon_{r,eff,dry}$
<i>E. coli</i>	-	6±1	3.3±0.4
<i>S. typhimurium</i>	-	7±1	4.7±1
<i>L. sakei</i>	+	19±5	3.3±0.6
<i>L. innocua</i>	+	18±7	3.7±0.7

Based on the equation 4-1, we used MatLab to indicate the relationship between CM factor and the electrical properties of the suspending particle and surrounding medium. We also calculated both the real part and imaginary part of the CM factor. The result was presented in the Fig. 4-1 and Fig 4-2.



(a)



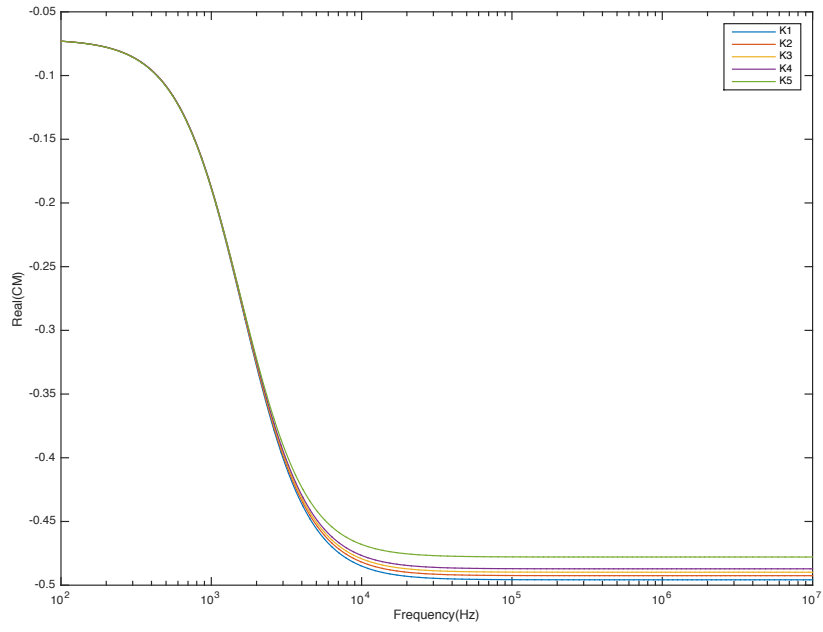
(b)

Fig. 4-1: CM factor for pathogens with different permittivity. Graphs K1, K2, K3 and K4 represent particles with permittivity 5, 8, 15 and 25, respectively and with the same conductivity as 0.031 mS/m. (a) real part of the CM factor and (b) Imaginary part of the CM factor.

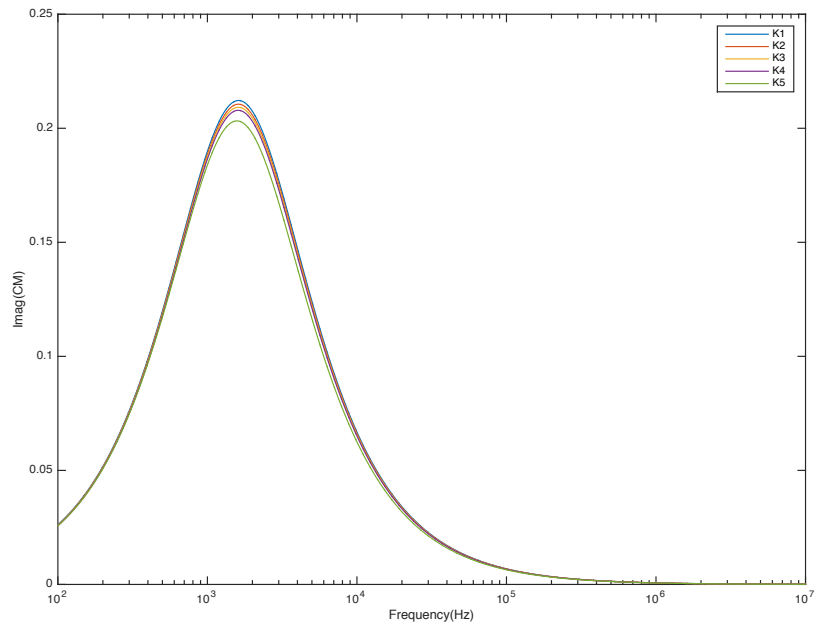
The four graphs K1, K2, K3 and K4 represent *E. coli*, *S. typhimurium*, *L. sakei* and *L. innocua*, respectively. Since the dielectric constants of *E. coli* and *S. typhimurium* are less than the dielectric constant of the medium, their starting values of the CM factor are less than zero. Similarly, Since the dielectric constants of *L. sakei* and *L. innocua* are greater than the dielectric constant of the medium, their starting values of the CM factor are greater than zero.

At low frequencies, the four graphs tend to be smooth and consistent with the condition of applying a DC electric field. As the frequency increases, the four graphs show a downward trend until the value of the CM factor drops to around -0.45.

In addition to studying the tendency of CM factors to change with the dielectric constant of bacteria, we also calculated the effect of particle conductivity on the CM factor. For this we used the same medium with permittivity and conductivity values of 10 mS/m and 55 mS/m respectively. Instead of changing the dielectric constant of the bacteria, we varied the conductivity of the pathogen while maintaining the same dielectric constant.



(a)



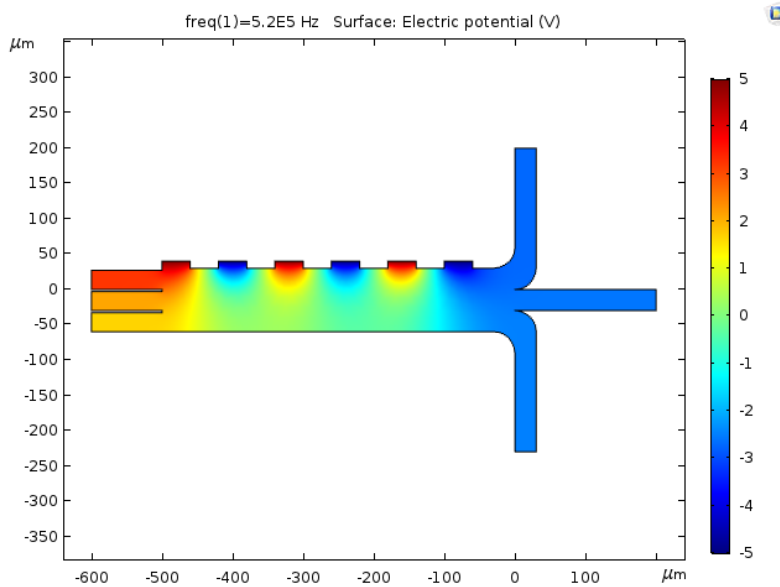
(b)

Fig. 4-2: CM factor for pathogens with different conductivity. Graphs K1, K2, K3, K4 and K5 represent particles with conductivity of 0.031 mS/m, 0.055mS/m, 0.075mS/m, 0.095mS/m and 0.31mS/m, respectively and have the same permittivity of 8. Variations of (a) real part of the Clausius-Mossotti (CM) factor and (b) Imaginary part of the Clausius-Mossotti (CM) factor.

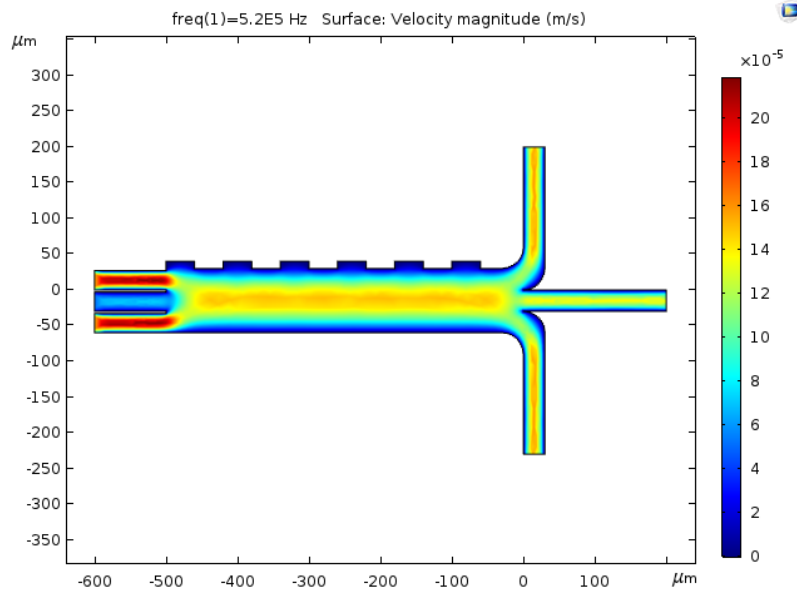
For same value of permittivity, the conductivity will not have too much effect on the CM) factor. The value of the CM factor is varied between -0.5–1 [31]. Based on this we can conclude that the magnitude of the DEP force mostly depends on the size of the bacteria and the magnitude of the electric field.

4.2 Separation Process

We designed our device to separate *S. typhimurium* mixed with other pathogens in aqueous medium. We first build a 2D device in order to determine the most appropriate frequency range which will maximize the DEP force. The test device device consists of 3 inlets channels, 3 outlets channels and a separation chamber in the middle. The electrode arrays were placed on the side of the separation chamber.



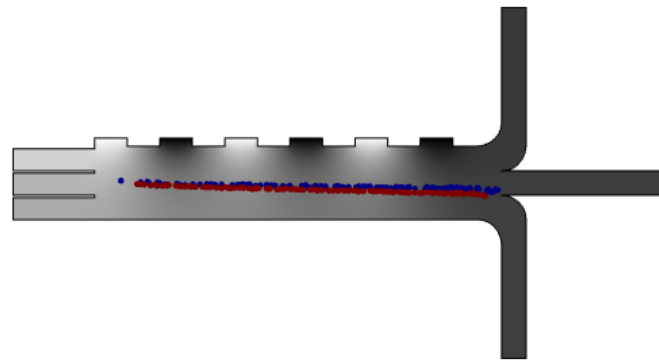
(a)



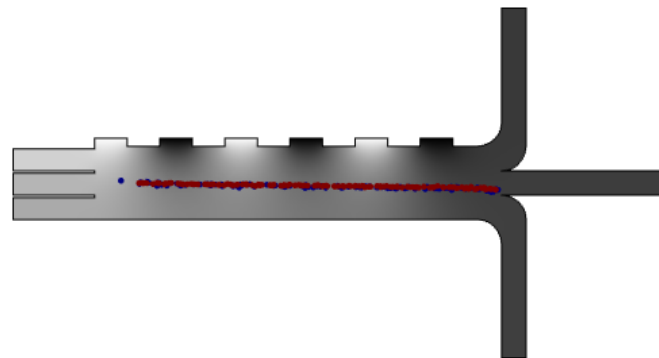
(b)

Fig. 4-3: 2D separation device showing (a) non-uniform electric field generated by the electrode array, (b) velocity of the fluid flow.

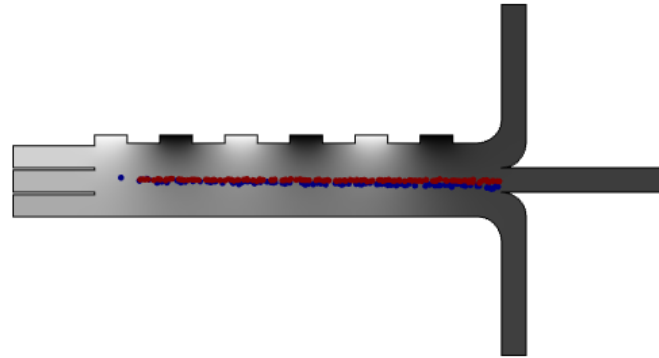
The mixed pathogen was injected into the device via inlet 1 located at the center while the medium was injected into the device via inlet 2 located at both sides of the device. We varied the frequency of the alternative current from 200 kHz to 520 kHz and finally found the reverse frequency (the frequency which will make the CM factor to become zero) of particle 2 are located around 480 kHz.



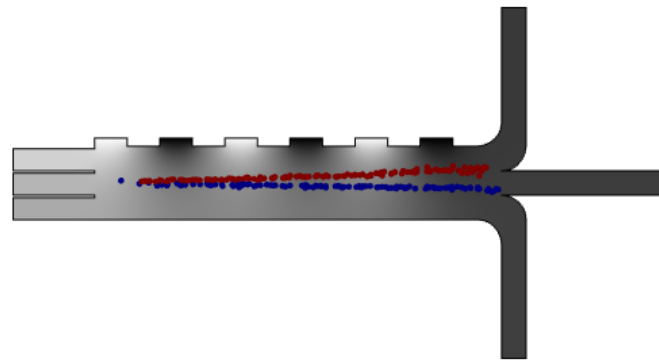
(a) $f=200$ kHz



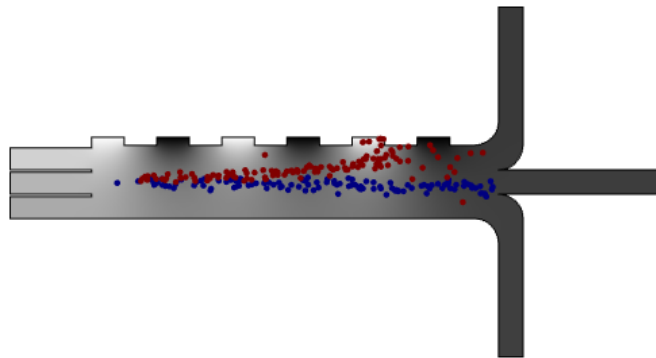
(b) $f=300$ kHz



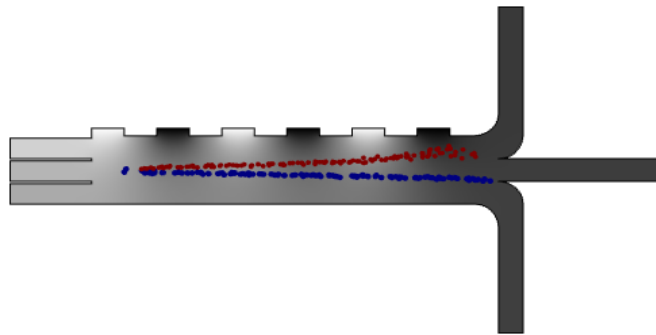
(c) $f=350$ kHz



(d) $f=400$ kHz



(e) $f=500$ kHz



(f) $f=520$ kHz

Fig. 4-4: Separation process for the testing device at different frequencies.

4.3 Device Modeling

Fig. 4-3 illustrates the structure of the chip. It consists of three inlet channels, one main chamber and three outlet branches. The task of the first separation zone is to isolate the particles in the mixed solution whose inversion frequency is lower than the target particle, and to discharge them towards outlet 1. The remaining of the mixed solution then continues to flow into the second separation zone where the particles have a reverse frequency greater than the target particle. This way the target particle is separated and removed from the outlet 3. The entire device contains two separate zones. The electrode array was placed on the side of the main channel and the electric current module was used to supply the alternative current. We used COMSOL Multiphysics software to model this fluid flow and with the particle tracking module to monitor the movement of the particles. Among others, one of the advantages of this chip is that we only need to determine the inverse frequency of our target cell. We varied the geometry parameters –length, depth and width of the channel one at a time, to see the parametric effect of particle separation on them.

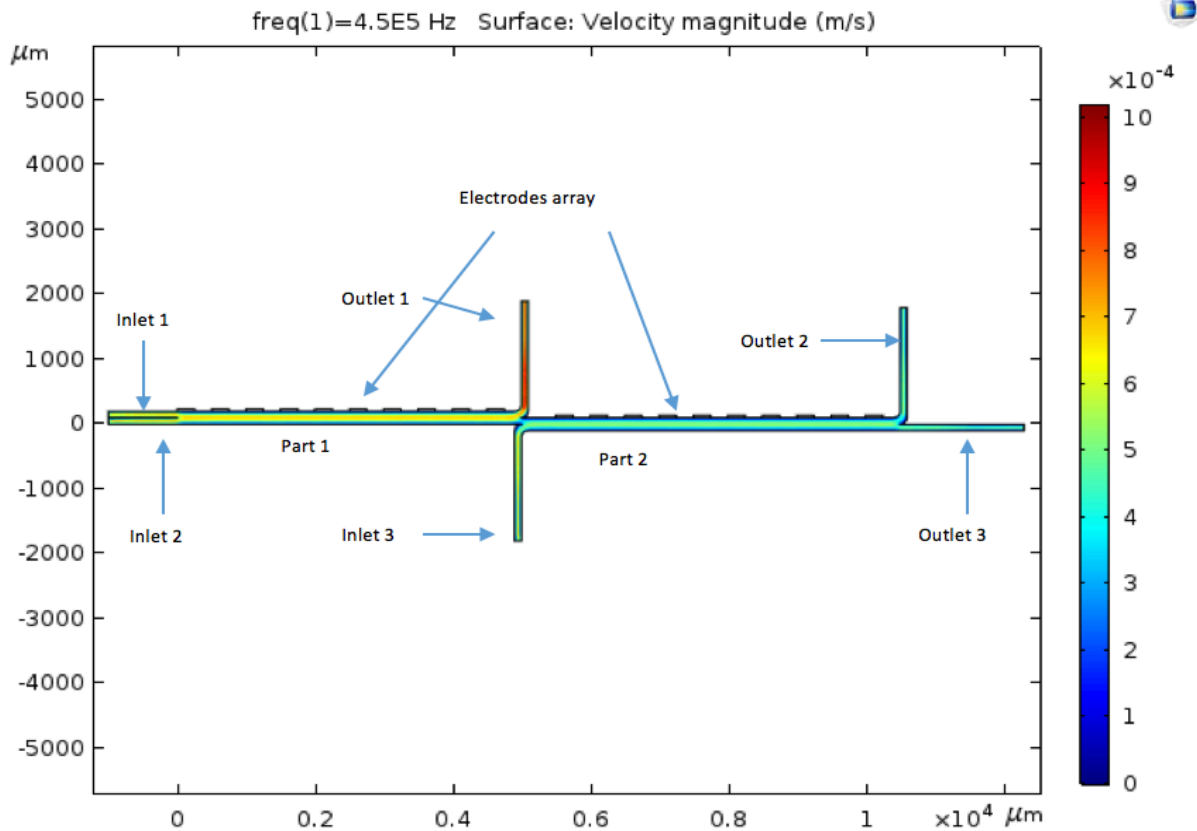
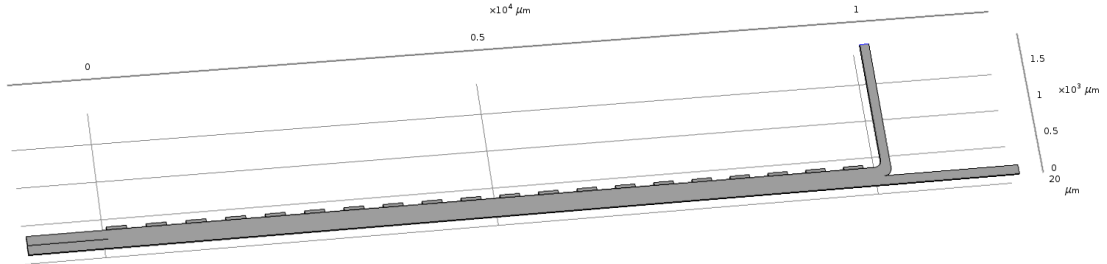


Fig. 4-5: Top view of the micro fluidic channel.

4.4 Separation Result for zone 1 of the Device

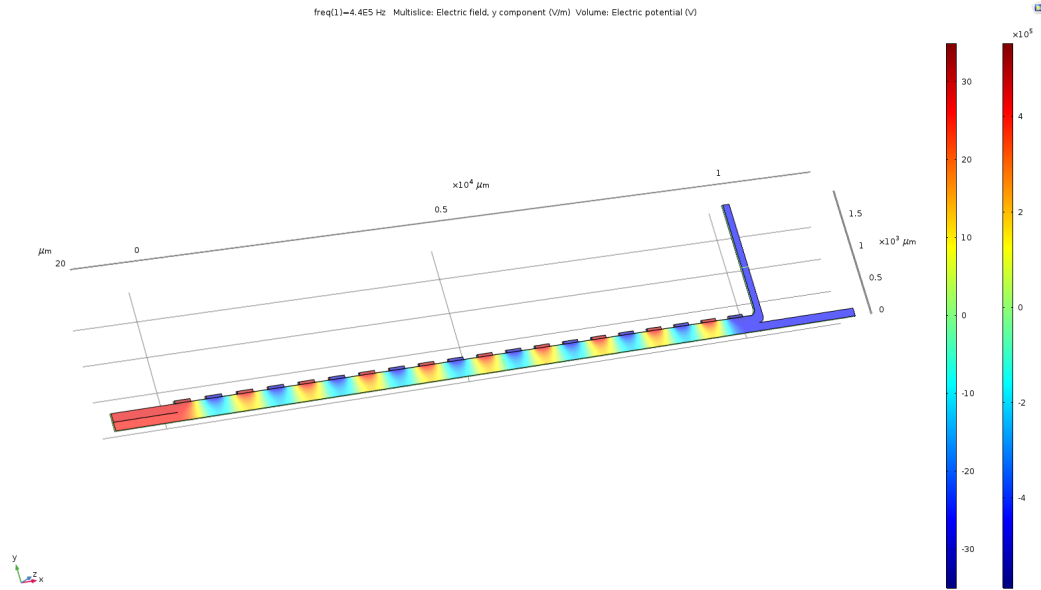
We mixed three different kinds of bacteria from inlet 3 with same concentration of 10000 cells/ml. Among them, the target pathogen *S. typhimurium* is labeled as particle 2. Another two pathogens are labeled as unknown particle 1 and unknown particle 3. The inflow velocity was set at $500\mu\text{m/s}$ for inlet 1 and $600\mu\text{m/s}$ for inlet 2. The electric current was oscillating at 440 kHz frequency at 35 V voltage. The width of the electrode array was $250\mu\text{m}$ and each of them was separated from each other by $250\mu\text{m}$.



(a)



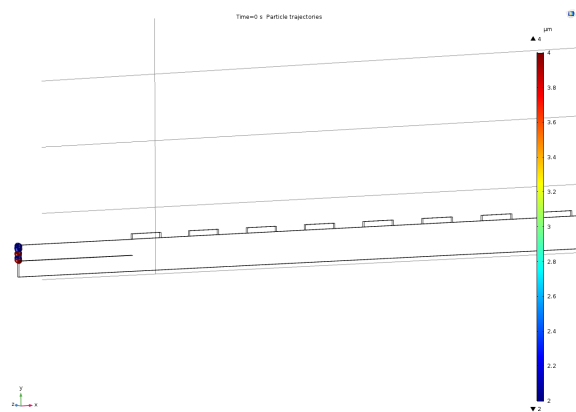
(b)



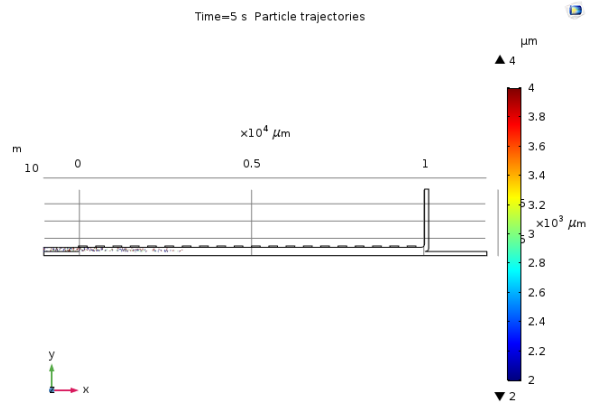
(c)

Fig. 4-6: Schematic of the zone 1 of the microfluidic device. (a) the geometry of the zone 1 of the chip. Contour of (b) the velocity of fluid flow. (c) the electric field generated by the alternative current.

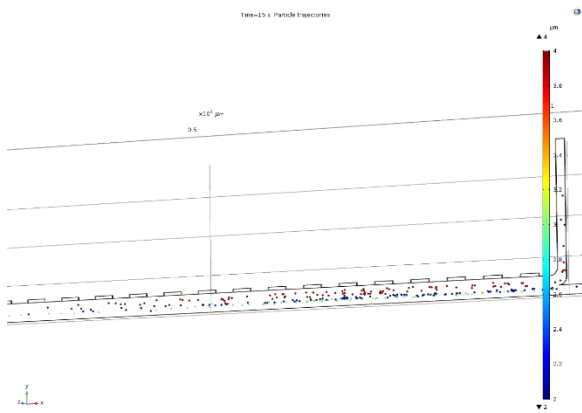
We varied the size of the device with depth from $20\mu\text{m}$ to $50\mu\text{m}$, length from $8000\mu\text{m}$ to $15000\mu\text{m}$ and width from $200\mu\text{m}$ to $320\mu\text{m}$. While flowing through the channel, particle 3 will face the positive DEP force and comes out from outlet1, particle 1 and particle 2 will face negative DEP forces and will move to the zone 2 of the device. We used particle counter to record the number of particles come at each outlet.



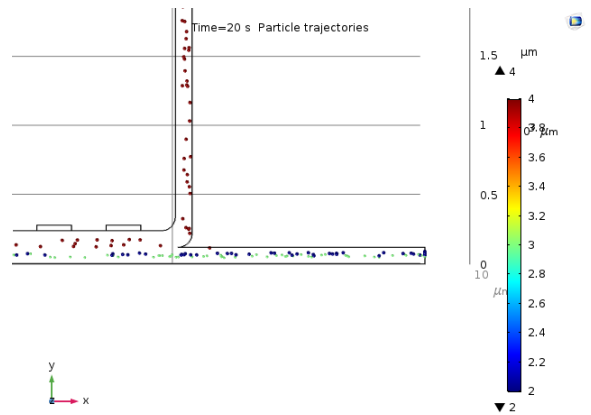
(a) $T = 0\text{s}$



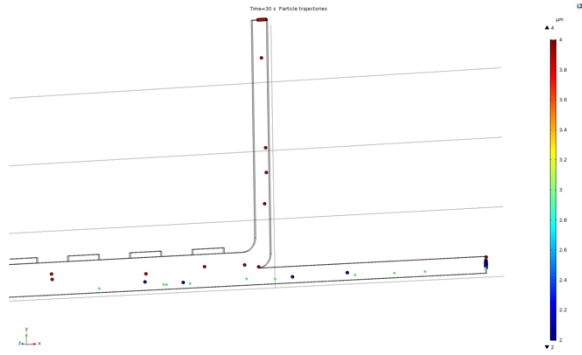
(b) $T = 5\text{s}$



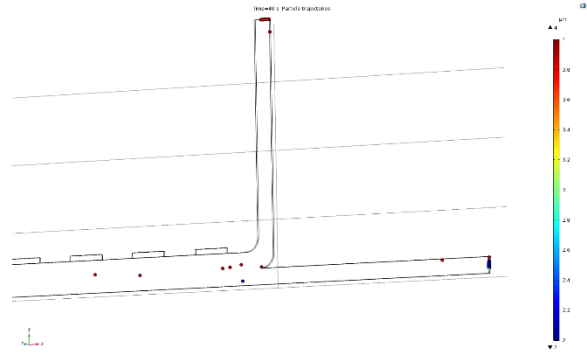
(c) $T = 15\text{s}$



(d) $T = 20\text{s}$



(e) T = 30s



(f) T = 40s

Fig. 4-7: Separation process in part 1 of the device with time at (a) 0s, (b) 5s, (c) 15s, (d) 20s, (d) 30s and (e) 40s, respectively.

After collecting the particles from each outlet, we calculated the separation rate of each type of particles. The result is presented in the table below.

Table 4-2: Performance of device with 10000 μm length and 240 μm width, while the channel depth varied between 20 μm to 50 μm .

DEPTH PARTICLE (μm)	DEPTH (μm)				
	50	40	30	20	
PARTICLE1+PARTICLE2	93.6	93.2	90.0	95.9	Separation Rate (%)
	3.6	6.8	10.0	4.1	Remain in Channel (%)
PARTICLE3	92.7	90.9	85.5	94.5	Separation Rate (%)
	5.9	7.3	9.1	5.5	Remain in Channel(%)

Table 4-3: Performance of device with 10000 μm length and 20 μm depth, while the channel width between 200 μm to 320 μm .

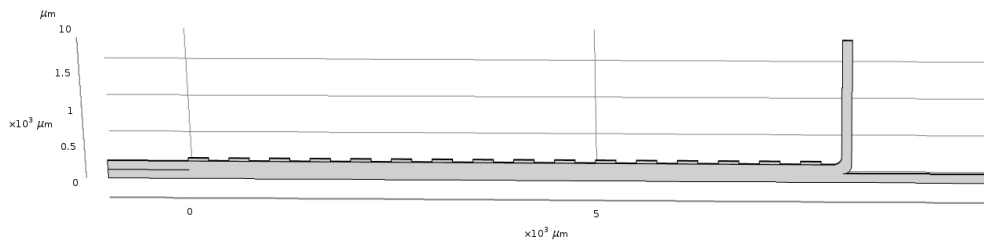
PARTICLE	WIDTH (μm)				
	320	280	240	200	
PARTICLE1+PARTICLE2	83.2	80.9	95.9	95.5	Separation Rate(%)
	10.9	19.1	4.1	4.5	Remain in Channel(%)
PARTICLE3	89.1	90.9	94.5	82.7	Separation Rate (%)
	10.9	9.1	5.5	9.1	Remain in Channel(%)

Table 4-4: Performance of device with 240 μm width and 20 μm depth, while the channel length varied between 8000 μm to 15000 μm .

PARTICLE	LENGTH (μm)				
	8000	10000	12000	15000	
PARTICLE1+PARTICLE2	95.9	95.9	92.3	91.8	Separation Rate(%)
	4.1	4.1	7.7	8.2	Remain in Channel(%)
PARTICLE3	91.8	94.5	83.6	73.6	Separation Rate (%)
	8.2	5.5	12.7	12.7	Remain in Channel(%)

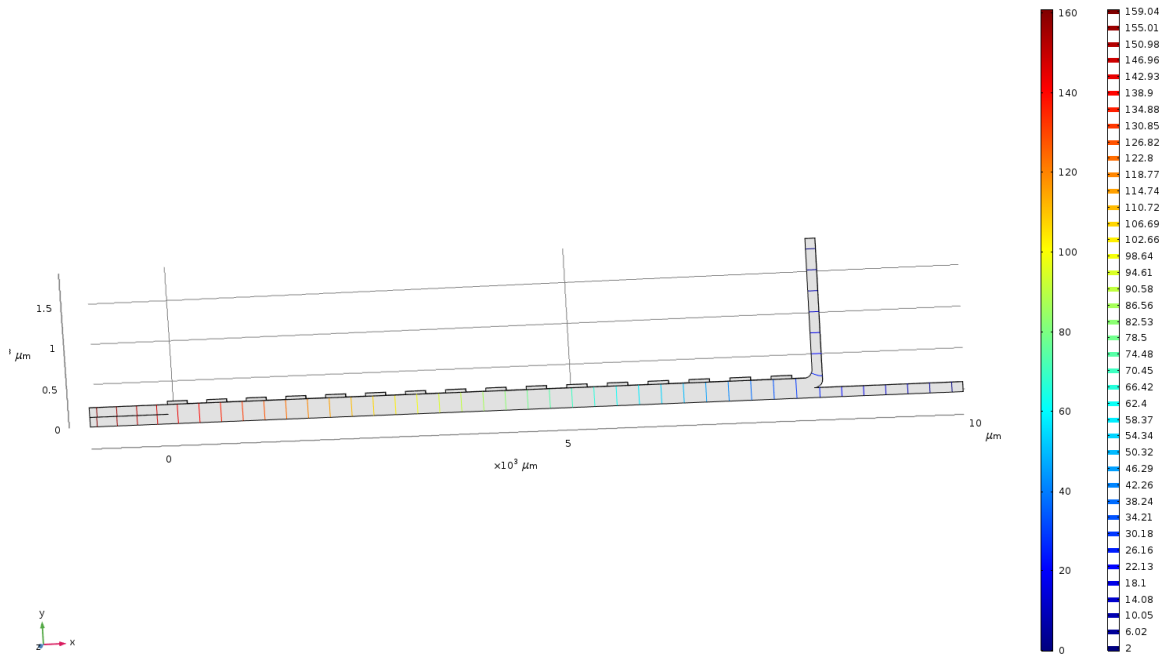
4.5 Separation Result for zone 2 of the Device

After the mixed solution passing through the zone 1 of the device, particle 3 will be isolated and flow out the channel via outlet 1 while particle 2 and particle 3 will keep flowing to the zone 2 of the device. For this, we set the frequency as 580 kHz and slightly increased the voltage applied to the electrodes to 40V. The target bacteria—particle 2 was collected from outlet 2 and the rest pathogen were flow out from outlet 3.



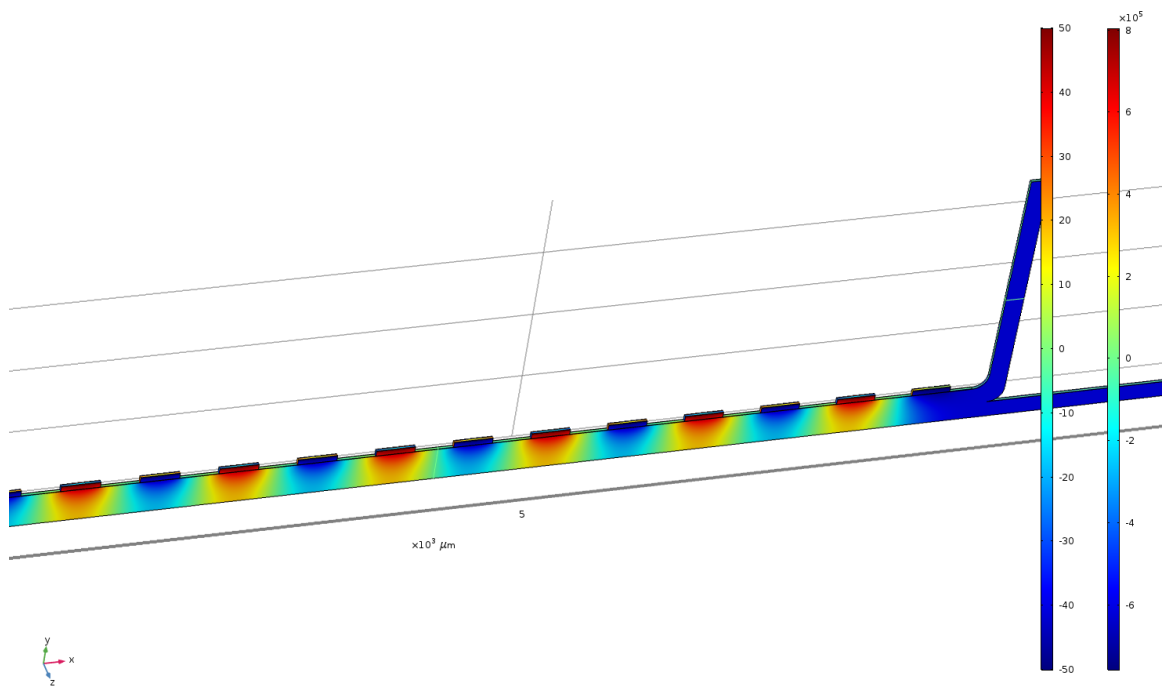
(a)

freq(1)=6ES Hz Contour: Pressure (Pa) Volume: Pressure (Pa)



(b)

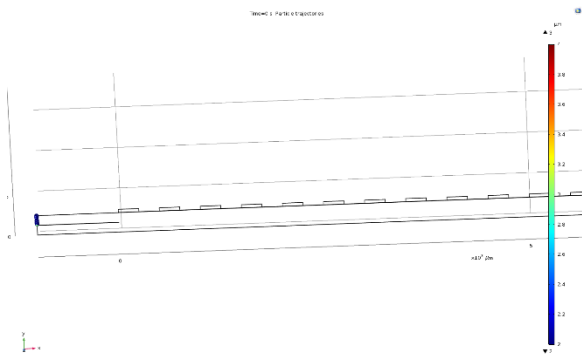
freq(1)=6ES Hz Multislice: Electric field, y component (V/m) Volume: Electric potential (V)



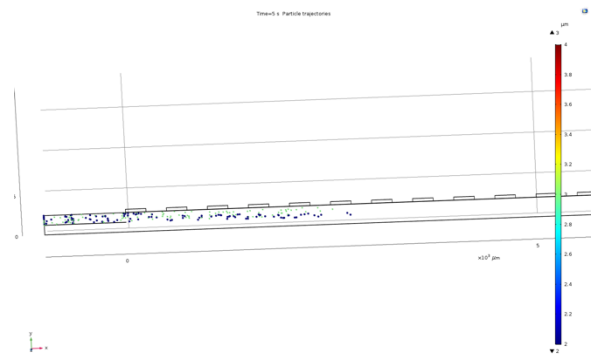
(c)

Fig. 4-8: Schematic of the zone 2 of the microfluidic device. (a) the geometry of the zone 2 of the chip. (b) The fluidic flow velocity of the cross area. (c) The electric field generated by the alternative current.

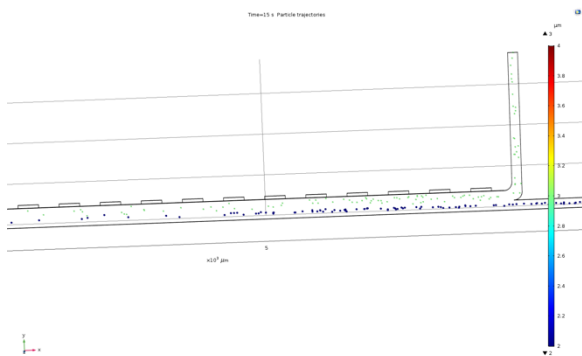
Similar to zone 1, we varied depth between $20\mu\text{m}$ to $50\mu\text{m}$, length between $8000\mu\text{m}$ to $15000\mu\text{m}$ and width between $200\mu\text{m}$ to $320\mu\text{m}$. The particle counter was placed at each outlet to record the number of particles collected at outlet 2 and outlet 3.



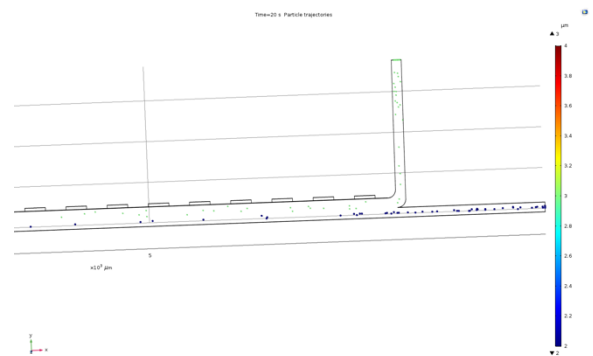
(a) $T = 0\text{s}$



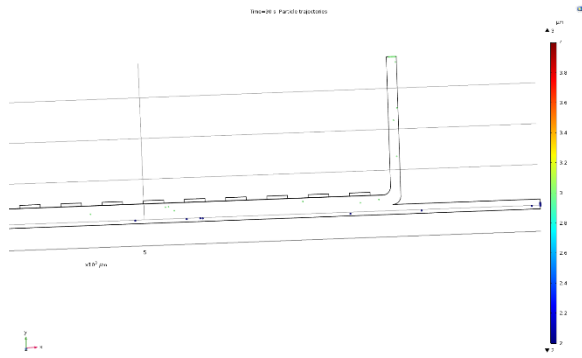
(b) $T = 5\text{s}$



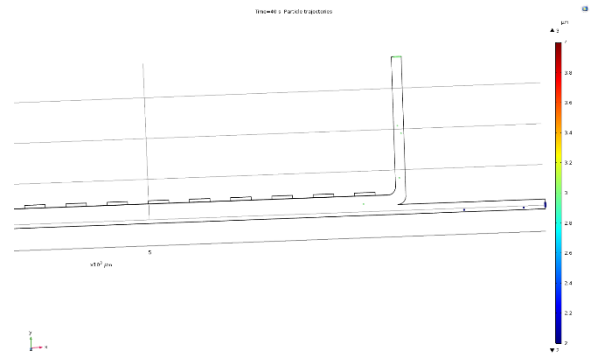
(c) $T = 15\text{s}$



(d) $T = 20\text{s}$



(e) T = 30s



(f) T = 40s

Fig. 4-9: Separation process in zone 1 of the device with time at (a) 0s, (b) 5s, (c) 15s, (d) 20s, (e) 30s and (f) 40s, respectively.

After collecting the particles from each outlet, we calculated the separation rate of each type of particles. The result is presented in the table4-7.

Table 4-5: Performance of device with 10000μm length and 240μm width, while the channel depth between 20μm to 50μm.

PARTICLE	LENGTH (μm)				
	8000	10000	12000	15000	
PARTICLE1	94.5	96.4	92.7	92.7	Separation Rate(%)
	5.5	3.6	7.3	7.3	Remain in Channel(%)
PARTICLE2	91.5	90.6	88.1	90.2	Separation Rate (%)
	18.2	30.0	30	34.5	Remain in Channel(%)

Table 4-6: Performance of device with 10000 μm length and 20 μm depth, while the channel width between 200 μm to 320 μm .

PARTICLE	WIDTH (μm)				
	320	280	240	200	
PARTICLE1	68.2	89.1	96.4	99.1	Separation Rate(%)
	10.0	10.0	3.6	0.9	Remain in Channel(%)
PARTICLE2	87.4	93.8	90.6	92.4	Separation Rate(%)
	21.8	31.8	30	34.5	Remain in Channel(%)

Table 4-7: Performance of device with 240 μm with and 20 μm depth, while the channel length between 8000 μm to 15000 μm .

PARTICLE	DEPTH (μm)				
	50	40	30	20	
PARTICLE1	96.4	91.2	91.2	96.4	Separation Rate(%)
	3.6	6.4	8.8	3.6	Remain in Channel(%)
PARTICLE2	84.3	80.5	92.3	90.6	Separation Rate (%)
	10.9	10.0	16.3	30.0	Remain in Channel(%)

CHAPTER V

DISCUSSION

5.1 Result Analysis

According to the result recorded in the chapter 4. The results show a very high separation rate for each trial. The reason why we observe the separation rate slightly decreased was when the length increase was there are more particle stick inside the channel and this can be improved by increase the flow time. Table 4-6 varied the channel width from 200 μm to 320 μm . We monitor the highest separation rate when we set the width between 280 μm and 200 μm . The other trials beyond this range does not match the size of the electrode array which will let the particles face too large or too small DEP force and cannot perfectly complete the separation process. Finally, Table 4-7 present the change of separation rate respect to different depth. Based on the result, we viewed that more particle will block inside the channel when the depth of the channel goes over than 30 μm (Fig. 5-1). This happened because the increase of the side wall area. Inside the micro fluid channel, the flow rate will heavily reduced when approached to the side wall, so larger side wall area will contain more particles and required more time to complete the separation process.

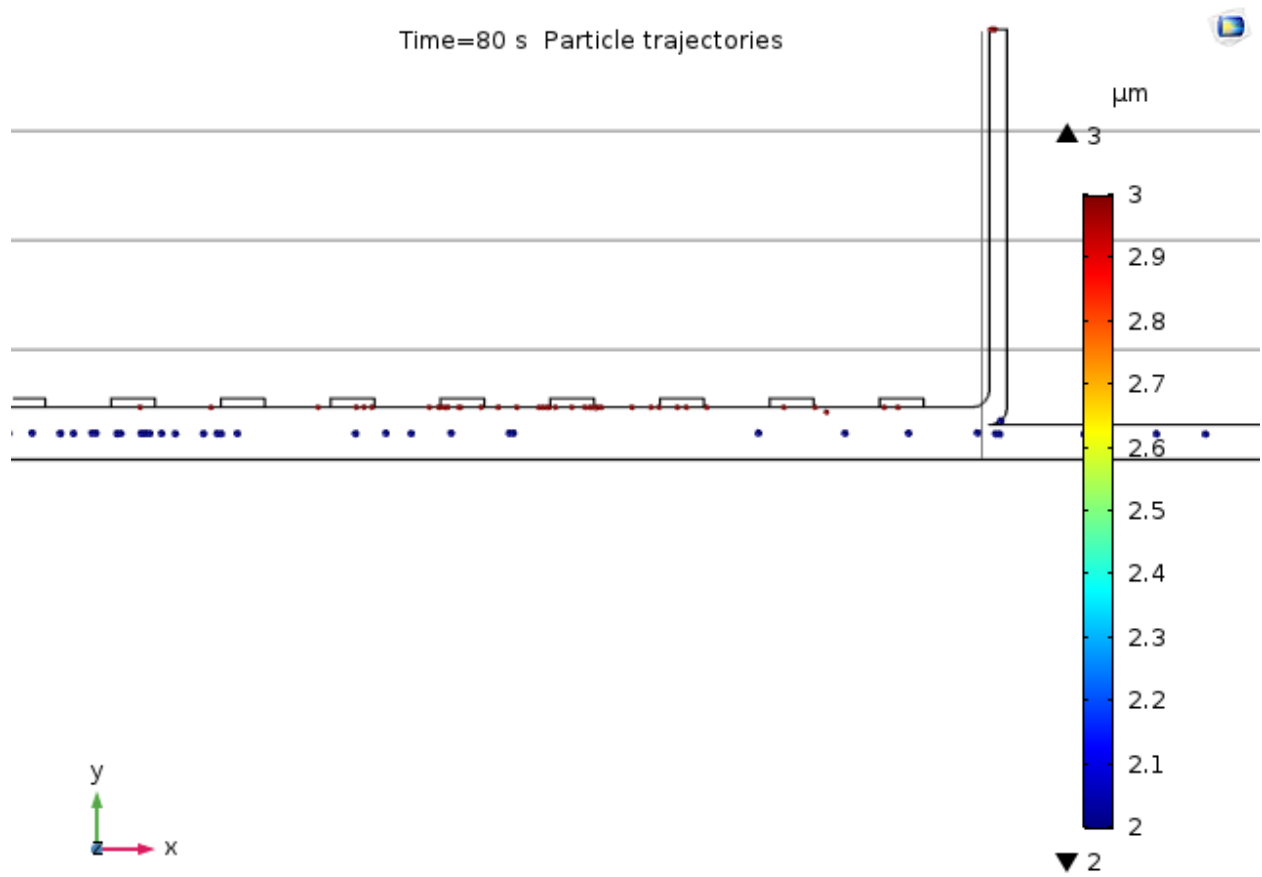


Fig. 5-1: Schematic diagram of how particles attracted by positive DEP force and stick on the electrode arrays.

5.2 Conclusion

Based on the data above we found out that most of the trials show high separation rate greater than 90%, especially when we build the device with 8000 μ m length, 240 μ m width and 20 μ m depth for both zone 1 and zone 2 will give us the best result. The final separation rate will be 95.1% for our target particle 2, the rest 4.9% were left inside the channel. We also summary the recent DEP separation chips which applied in other cells and present their result in the table 5-1.

Table 5-1: Recent DEP separation chip application.

APPLICATION	TARGET CELL	SEPARATION RATE (%)	PROCESS TIME	REFERENCE
Real-Time based PCR	<i>E. coli</i>	NA	5 h 20 min	[37]
Combined DEP and impedance system for on-chip controlled bacteria concentration	<i>E. coli</i>	85.65 \pm 1.07%	10 min	[38]
Continuous cell separation chip using hydrodynamic DEP process	Viable yeast	95.9%-97.3%	NA	[23]
	Nonviable yeast	64.5%-74.3%		

In conclusion our device maintains high separation rates while handling complex mixed solutions. Most important, each isolated particle have very high purity > 95%. What's more, we can improve the separation result by reduce the voltage, increase the flow rate and switch the AC electrical signal as a pulse with some duty ratio [23]. But this will increase the operating time which need us to increase the length of the channel.

5.3 Summary

With the development of science and technology, the links between various disciplines have become more and more close. Many interdisciplinary applications have brought many unexpected effects to humans. A DEP-based pathogen separation and detection chip is one of the most typical representatives. By introducing physical and engineering techniques, the traditional complex and time-consuming process of detecting bacteria has become much easier. At the same time, this technology has great potential for improvement. By further introducing detection techniques such as Raman spectroscopy, the entire detection process can be made faster and more accurate.

5.4 Future Work

Our future work is mainly focused on two aspects:

(1) Considering that the shape of *S. typhimurium* is roughly a cylinder, we will build a more complex bacterial model to make the simulation closer to reality.

(2) Fabricate the microfluidic device. We are trying to use the polymer materials include polydimethylsiloxane (PDMS) to fabricate the microfluidic chip, then bond it on the silicon or glass substrate. PDMS is a colorless and transparent viscous liquid with good chemical stability, low freezing point, good hydrophobic properties and high shear resistance. Because PDMS also

has good biocompatibility, thermal stability (up to 186 °C in air) and non-toxic characteristics, it is often used to manufacture microfluidic chips [39]. The entire microfluidic chip manufacturing process is usually divided into three parts: lithography, etching and bonding. Also, in order to minimize the contamination from the dust and airborne particles, a cleanroom is required to manufacture the microelectromechanical systems (MEMS).

CHAPTER VI

ELECTROPORATION

6.1 Introduction

Interdigitated microelectrodes can also be used as an electroporation chip. Electroporation, as literally, temporarily changes the permeability of the cell membrane by applying short and energetic electric field across it. Although this phenomenon was first observed by Nollet [40] in the mid-18th century, it was not until 1980 that Neumann [41] applied this technique in the field of medicine. In the following decades, electroporation has been widely used to deliver foreign macromolecules into cells. Since electroporation does not cause mechanical damage to the cells, and the lipid bilayer structure of the cell membrane can be restored, therefore, the cells can remain viable during the process.

6.2 Fundamental Principles

Under normal circumstances, the cell membrane does not allow the current to pass through which will make it act as an electrical capacitor. Therefore, applying a high-intensity electric field to the cell membrane will result in the aqueous pores formed on the membrane. When the applied external electric field is suitable, enough pores can be generated and more stable to obtain a longer lifetime. Electroporation is a dynamic phenomenon that depends on the local transmembrane voltage at each point on the cell membrane. The transmembrane potential [42] induced in a cell by an external electric field is given by the equation:

$$\Delta V_m = f E_{ext} r \cos \phi \quad (6-1)$$

Where ΔV_m is the transmembrane potential, f is a form factor describing the impact of the cell on the extracellular field distribution, E_{ext} is the applied electric field, r is the cell radius and ϕ is the polar angle with respect to the external field. Although, the value of the factor f is dependent on a number of different factors [42], under physiological conditions many authors list it as 1.5. When the ΔV_m superimposed on the resting transmembrane potential is larger than a threshold, electroporation is achieved. Compare to all other available technologies, electroporation has some unique advantages in primary cells transfection.

6.3 Electroporation Chip

The electroporation chip was designed to supply the external electric field on cells. It consists of an interdigitated metal electrodes (IME) and a PCL (Polycaprolactone) nanofiber membranes. Metal electrodes made of Au thin films on top of Ti adhesion layer on a glass substrate were used to apply the electric field. Metal electrodes were fabricated using liftoff technique in the cleanroom. PCL nanofiber membranes were constructed using an electrospinning apparatus, which provided the structural basis to which the cells remain adhered during the electroporation.

6.3.1 Electroporation Chip Design

The electroporation chip was designed using IntellisuiteTM finite element analysis software. 32 different types of electroporation chips were designed. Keeping the area occupied by each chip same (17 mm X 17 mm), the number of electrodes lines and mutual distance between adjacent electrodes were varied to see their effect on electroporation. The number of electrode lines was varied from 5 to 12 and the width of the lines from 25 to 200 μm while with the distance between electrode lines ranging from 0.63 to 2.19 mm. The designed electrodes are shown in Fig. 6-1

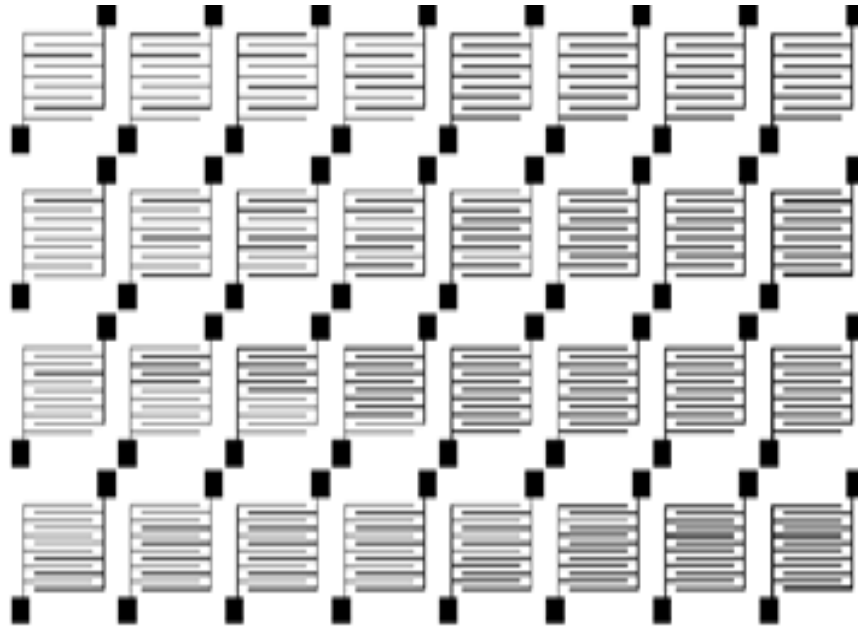


Fig. 6-1: Layout of the photomask containing 32 different designs of electrode lines

6.4 Fabrication Process

The photolithography and liftoff techniques are the most common ways used in electrode array fabrication. Optical photolithography uses ultraviolet light to accurately transfer or replicate the geometric pattern from photomask to a light sensitive chemical ‘photoresist’, which is coated on the surface of a target substrate. There are two kinds of photoresists used for different applications- in the case of positive photoresist, the chemical material will be degraded when exposed to light and can be easily dissolved away using the photoresist developer. In the case of negative photoresist, the chemical material will be strengthened when exposed to light and the unexposed part can be dissolved away by using developer. The advantage of positive photoresist is that the precision of the replica is high, and the advantage of the negative photoresist is durability. The fabrication process generally includes three steps: photolithography, deposit, and liftoff.

Fig. 6-2 illustrates the process of photolithography. The first step needed is to prepare a clean glass substance and coat the photoresist on the substrate via spin coating machine. The thickness of the photoresist layer depends on the spin speed. After that, the coated substrate is baked at 90°C for a minute to drive the solvent out of the resist. In following step, we placed the coated substrate and photomask on the alignment machine to align, then exposed it under ultraviolet (UV) light. The photomask is a square plate made of glass or quartz with a specific chromium pattern layer covered on top. When doing exposure, the chromium pattern will reflect the UV light while the rest area will allow UV light to penetrate through the photomask. The last step for photolithography is develop. We immersed the chip into the developer to wash off the photoresist. In case of positive photoresist, the developer can remove the exposed regions. In contrast, for negative photoresist, the developer can remove the unexposed regions. After developing the positive from Shipley, the geometry pattern was precisely transferred from photomask to photoresist.

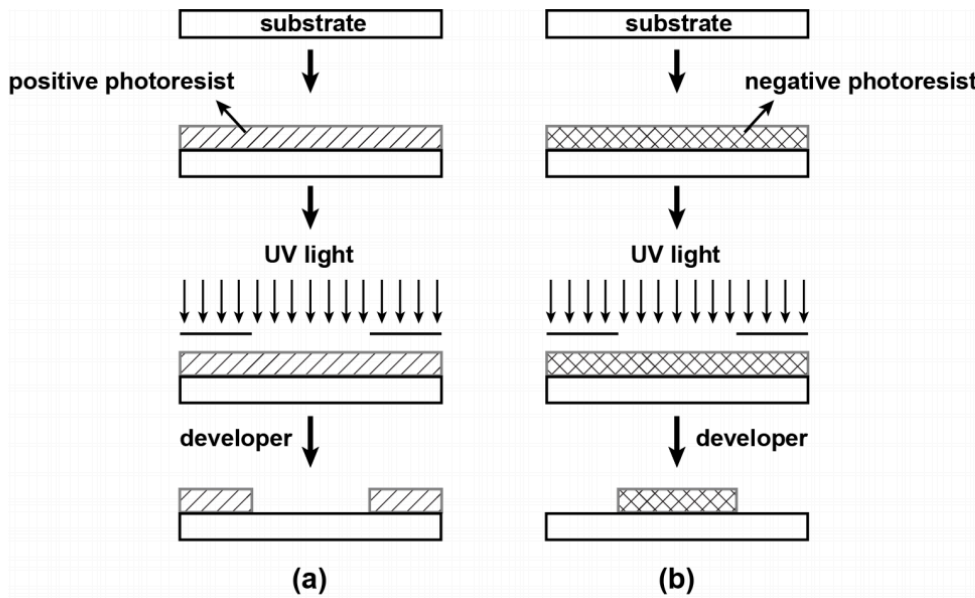


Fig. 6-2: Steps of photolithography process. (a) Positive photoresist. (b) Negative photoresist.

The next step was to deposit the metal on top of the developed chip to form the electrode lines. The process was done by a sputtering machine, we placed the chip faced up inside the vacuum chamber and pump it down to a pressure of $\sim 10^{-6}$ torr. The electrode lines were made of radio frequency (RF) sputtered gold (50 nm) on top of 500 nm thick Ti which was also deposited by RF sputtering. Both Ti and Au layers were deposited together on top of photoresist processed in previous step.

The last part is liftoff. We used acetone to dissolve the rest of photoresist remained on the glass substrate and the metal lies on top of the photoresist striped off as well. After photoresist was completely dissolved by acetone, the fabrication process for the electroporation chip is done. Figure 6-3 shows the lift off process, while Figure 6-4 shows the camera picture of the fabricated chip.

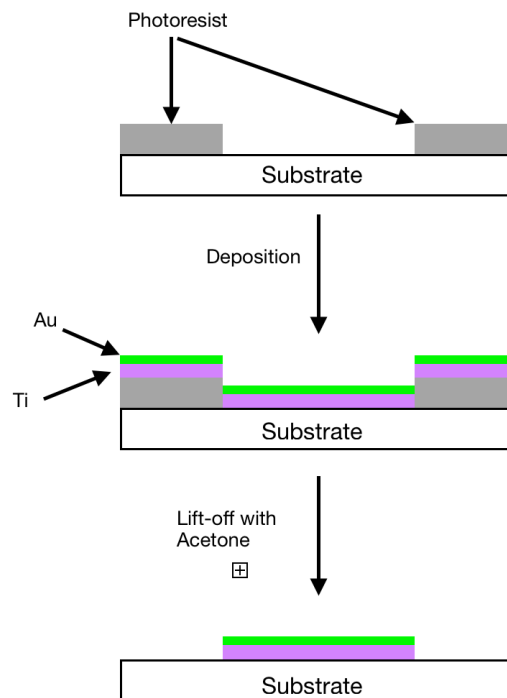


Fig. 6-3: An illustration of lift-off process



Fig. 6-4: Photograph of an actual chip aligned with PCL nanofiber

CHAPTER VII

EXPERIMENT SETUP RESULTS FROM ELECTROPORATION

7.1 Cell Preparation

The chicken embryo optic tectum neurons were stripped out from the 7-day-old fertilized egg. We removed the pial membrane which was wrapping around the optic tectum and placed it into cold Hanks' balanced salt solution (HBSS). Then, it was diced into small pieces with a spring scissors. In the next step, we collected the pieces into a 15 ml conical tube and removed as much of the HBSS as possible after letting the pieces sank. We added 1ml of *TrypLE Express* solution and incubated that at 37⁰C for 15 minutes. After incubation, the TrypLE were carefully removed without disturbing the chunks and 1 ml neuron culture medium was added to supply the nutrition. The solution was standing for a while until the pieces sank to the bottom and the medium was carefully removed after that. We repeated this step one more time to wash off the trypsin. In the following step, we added 2 ml of neuron culture medium and started triturating. Trituration involved taking a sterile fire-polished Pasteur pipette and the tissues were passed through it several times gently until there were no more chunk left. In the last step, we needed to count viable cells using Trypan Blue dye and the Hemacytometer. The resuspended cells were diluted in a ratio of 1:10 (10 μ l cells + 90 μ l of neuron culture medium). We took 50 μ l of the diluted cells to 1.5ml centrifuge tube and added 50 μ l of Trypan Blue solution. After placing the coverslip, the hemacytometer was used to count the bright clear cells. If the cells are dyed blue by the reagent, means those cells were died and should not be counted.

7.2 Chip Preparation

During the incubation, we prepared the electroporation chip with Matrigel. Matrigel is extracellular matrix and used to immobilize the cells on top of the electroporation chip. We used Matrigel diluted to 25% in dulbecco's modified eagle medium (DMEM). In the first step, we sterilized the chips with 95% ethanol thoroughly and left to dry in the BSL2 hood. When the chips were completely dry, we quickly took 50 μ l of diluted Matrigel and added that to the center of the chips. The diluted Matrigel were spread to cover as much area of the chips as possible with the pipette tip. Immediately after, we took off it with the same pipette tip and returned it to the tube on ice. The goal of this process was to leave a thin film of Matrigel solution to polymerize. When the chips were well prepared, we placed them in plate, covered with lid and keep it in the 37°C CO₂ incubator until they were ready to implant the cells.

7.3 Electroporation

We lined the chip with PCL nanofiber which was adhered by silicone gel. The cells were implanted on the prepared chips. We placed the chips back to the 37°C CO₂ incubator for 24 hours until the cells were fully immobilized. After 24 hours of incubation, the cells were electroporated following the addition of DNA using the electroporator - Electrosquare Porator ECM830. The cells were observed after 96 hours of electroporation under a fluorescence microscope. The cells which were electroporated fluoresced due to the permeation of DNA.

7.4 Result

We inspected the cells under the fluorescence microscope. Successful electroporation result in the cells to express GFP (green fluorescence protein) plasmid. The result captured by camera is presented in the Fig. 7-1.

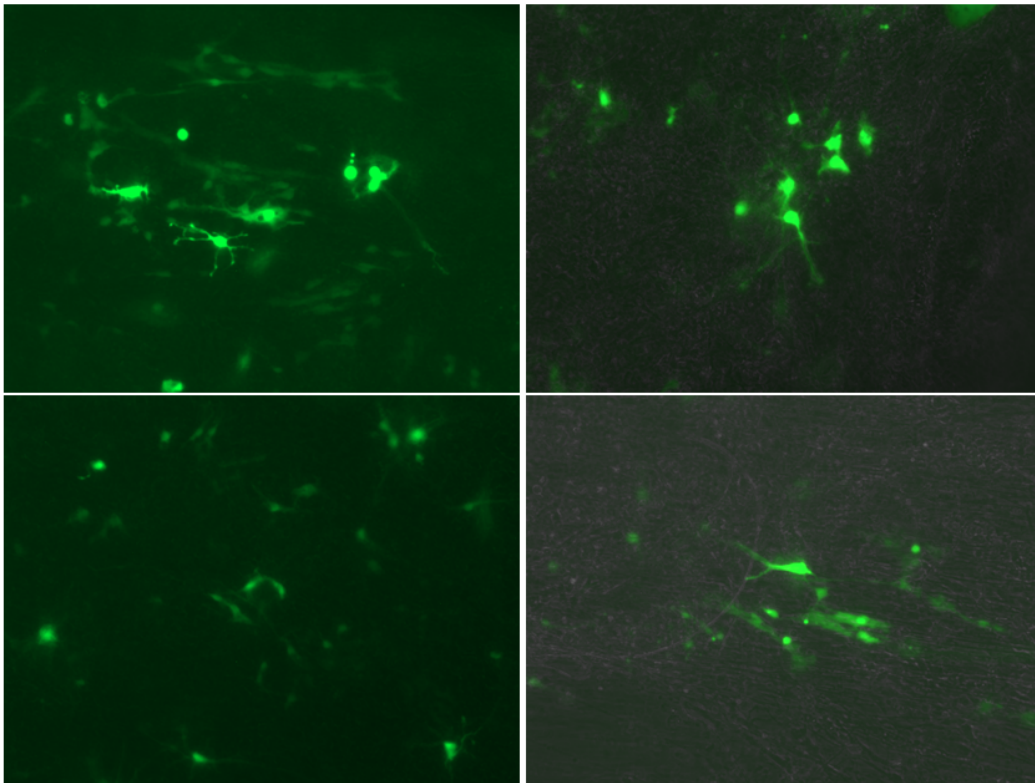


Fig. 7-1: GFP plasmids is delivered into using the electroporation chip and expressed in chicken embryo optic-tectum cells.

7.5 Conclusion and Future Work

Fluorescence pictures from Fig 7-1 confirms that electroporation had occurred and the definite shape of the cells implies that the cells are alive and healthy. The cells are supported by the

nanofiber scaffolds. The efficiency of electroporation can be varied by changing the pulse length, amplitude and number of pulses.

The aim of the experiment was to obtain the electroporation of the cells for DNA transfer without damaging the cells. Our future work will focus on manipulate the electric field to find the property pulse frequency and strength. The strength of the electric field can be classified into four ranges corresponding to the performance of the cells [43]: (1) No detectable electroporation: This is the lowest strength range, under this range of strength no molecular can be transferred. (2) Reversible electroporation: This is the most suitable strength range, under this range the pathway for DNA transport are temporarily formed. After turning off the electric pulse, the cells' membrane will restore quickly, close the pathway and remain the cells viable. (3) Nonthermal irreversible electroporation: Within this strength range, although the cells have not been thermally damaged, the cells are hardly to recover the membrane. This eventually result in the death of the cells. (4) Irreversible electroporation accompanied by thermal effects: This is the highest strength range which will the cause the temperature significantly increased and kill the cells.

The aim of our future is to find the most appropriate electric field strength, observe the effect of thermal damage and determine the electroporation efficiency.

References

- [1] "Reducing the risk from *E. coli* 0157 – controlling cross-contamination," Food Standards Agency, United Kingdom. February 2011.
- [2] Dwivedi H.P., and Jaykus L.A. "Detection of pathogens in foods: The current state-of-the-art and future directions," *Crit. Rev. Microbiol.* 2011, 37, 40–63.
- [3] Alahi MEE., and Mukhopadhyay SC. " Detection Methodologies for Pathogen and Toxins: A Review," *Sensors* 17(8): 1885 (2017). [j20].
- [4] Mullis, K.B.; Erlich, H.A.; Arnheim, N.; Horn, G.T.; Saiki, R.K.; Scharf, S.J. . "Process for amplifying, detecting, and/or-cloning nucleic acid sequences" U.S. Patent. 1989. Web.
- [5] Weiland G. "The enzyme-linked immunosorbent assay (ELISA)--a new serodiagnostic method for the detection of parasitic infections (author's transl)," *MMW Munch Med Wochenschr*
- [6] Leoni, E.; Legnani, P.P. "Comparison of selective procedures for isolation and enumeration of legionella species from hot water systems," *J. Appl. Microbiol.* 2001, 90, 27–33.
- [7] Sharkey, D. J.; Scalice, E. R.; Christy, K. G.; Atwood, S. M.; Daiss, J. L. "Antibodies as Thermolabile Switches: High Temperature Triggering for the Polymerase Chain Reaction". *Bio/Technology*. 1994.
- [8] Chien A, Edgar DB, Trela JM, "Deoxyribonucleic acid polymerase from the extreme thermophile *Thermus aquaticus*". *J.Bacteriol.* 1976. PMC 232952. PMID 8432.
- [9] Lawyer, F.; Stoffel, S.; Saiki, R.; Chang, S.; Landre, P.; Abramson, R.; Gelfand, D. "High-level expression, purification, and enzymatic characterization of full-length *Thermus aquaticus* DNA polymerase and a truncated form deficient in 5' to 3' exonuclease activity". *PCR Methods and Applications*. 1993. PMID 8324500

- [10] Enzoklop. "Wikimedia, Schematic drawing of the PCR cycle"
https://commons.wikimedia.org/wiki/File:Polymerase_chain_reaction.svg. 5 April 2014
- [11] Spence, Zachary (2018-10-18). "Biochemistry 8th ed - Jeremy M. Berg": 83. ^ Schmidt, SD; Mazzella, MJ; Nixon, RA; Mathews, PM (2012).
- [12] Madhukar Varshneya, Yanbin Lib, " Interdigitated array microelectrodes based impedance biosensors for detection of bacterial cells," Biosensors and Bioelectronics. Volume 24. 2009.
- [13] Shibajyoti Ghosh Dastider,¹ Syed Barizuddin,² Nuh S. Yuksek,¹ Majed Dweik,² and Mahmoud F. Almasri¹, " Efficient and Rapid Detection of Salmonella Using Microfluidic Impedance Based Sensing" Journal of Sensors, vol. 2015, Article ID 293461, 8 pages, 2015. <https://doi.org/10.1155/2015/293461>.
- [14] Kirby, B.J. "Micro- and Nanoscale Fluid Mechanics: Transport in Microfluidic Devices." Cambridge University Press. 2010.
- [15] Karniadakis, G.M., Beskok, A., Aluru, N. "Microflows *and* Nanoflows." Springer Verlag. 2005
- [16] CENTER FOR FOOD SAFETY, Cristina R. Stella, Case 2:13-cv-00679-RJS
- [17] Niccolò Piacentini, Guillaume Mernier, Raphaël Tornay, and Philippe Renaud. "Separation of platelets from other blood cells in continuous-flow by dielectrophoresis field-flow-fractionation," Biomicrofluidics. Sep 5, 2011.
- [18] Nurhaslina Abd Rahman, Fatimah Ibrahim, and Bashar Yafouz. "Dielectrophoresis for Biomedical Sciences Applications: A Review" Sensors. 2017.
- [19] Nicole Pamme. "Continuous flow separations in microfluidic devices" Lab on a Chip. 2007. DOI:10.1039/b712784g.

- [20] Herold, KE; Rasooly, "Lab-on-a-Chip Technology: Fabrication and Microfluidics." Caister Academic Press. 2009. ISBN: 978-1-904455-46-2.
- [21] H.A. Pohl, "The motion and precipitation of suspensoids in divergent electric fields," J. Appl. Phys., 22 (1951) 869-871.
- [22] Jones T. B. "Electromechanics of Particles. Cambridge University Press." 1995. ISBN: 978-0521019101.
- [23] R. Pethig, "Review Article-Dielectrophoresis: Status of the theory, technology, and applications," Biomicrofluidics, 4 (2010) 022811.
- [24] Il-Doh, Young-Ho Cho, "A continuous cell separation chip using hydrodynamic dielectrophoresis (DEP) process" Sensors and Actuators A: Physical. Volume 121. 2005.
- [25] Jones T. B. " Electromechanics of Particles." Cambridge University Press. 1995. ISBN: 978-0521019101.
- [26] Morgan, Hywel; Green, Nicolas G. "AC Electrokinetics: Colloids and Nanoparticles." Research Studies Press. 2003. ISBN: 9780863802553.
- [27] Irimajiri, Akihiko; Hanai, Tetsuya; Inouye, Akira, "A dielectric theory of "multi-stratified shell" model with its application to a lymphoma cell". Journal of Theoretical Biology. 1979. 78 (2): 251–269. doi:10.1016/0022-5193(79)90268-6.
- [28] I-Fang Cheng¹, Hsien-Chang Chang², Tzu-Ying Chen¹, Chenming Hu³ & Fu-Liang Yang¹, "Rapid (<5 min) Identification of Pathogen in Human Blood by Electrokinetic Concentration and Surface-Enhanced Raman Spectroscopy." Scientific Reports. Volume 3. Article number: 2365 (2013)

- [29] Ronald Pethig (1996), "Dielectrophoresis: Using Inhomogeneous AC Electrical Fields to Separate and Manipulate Cells," *Critical Reviews in Biotechnology*, 16:4, 331-348, DOI: 10.3109/07388559609147425
- [30] Giddings, JC, FJ Yang, and MN Myers. "Flow Field-Flow Fractionation: a versatile new separation method." *Science* 193.4259 (1976): 1244–1245.
- [31] Niccolò Piacentini, Guillaume Mernier, Raphaël Tornay, and Philippe Renaud. "Separation of platelets from other blood cells in continuous-flow by dielectrophoresis field-flow-fractionation". *Biomicrofluidics*. Sep 5, 2011.
- [32] Wang L1, Flanagan LA, Monuki E, Jeon NL, Lee AP. "Dielectrophoresis switching with vertical sidewall electrodes for microfluidic flow cytometry," *Lab Chip*. 2017. PMID 17713608
- [33] Peter Gascoyne,a,* Jutamaad Satayavivad,b,c and Mathuros Ruchirawatb,c."Microfluidic approaches to malaria detection" *Acta Trop*. 2004 Feb; 89(3): 357–369.
- [34] Yuejun Kang. "On-chip separation and detection of biological particles using dielectrophoresis and resistive pulse sensing" PhD Thesis. Vanderbilt University. 2008.
- [35] Daniel Esteban-Ferrer, Martin A. Edwards, Laura Fumagalli, Antonio Juárez, and Gabriel Gomila, "Electric polarization properties of single bacteria measured with electrostatic force microscopy," *ACS Nano*. 2014. DOI: 10.1021/nn5041476
- [36] Ali Zifan, "Wikimedia, A diagram of a typical prokaryotic bacteria cell." 12 October, 2015.
- [37] Fu,Z.;Rogelj,S.;Kieft,T.L. " Rapid detection of *Escherichiacoli* O157:H7 by immunomagnetic separationand real-time PCR." *Int. J. Food Microbiol*. 2005.
- [38] Schröder U.-C., Ramoji A., Glaser U., Sachse S., Leiterer C., Csaki A., Hübner U., Fritzsche W., Pfister W., Bauer M., "Combined Dielectrophoresis–Raman Setup for the Classification of Pathogens," *Chem*. 2013.

- [39] H. Hillborg; J.F. Ankner; U.W. Gedde; G.D. Smith; H.K. Yasuda; K. Wikstrom (2000). "Crosslinked polydimethylsiloxane exposed to oxygen plasma studied by neutron reflectometry and other surface specific techniques". *Polymer*. 41 (18): 6851–6863. doi:10.1016/S0032-3861(00)00039-2.
- [40] Nollet JA., "Recherches sur les causes particulieres des phénomènes électriques." Paris: Guerin & Delatour.1754.
- [41] Neumann, E; Schaefer-Ridder, M; Wang, Y; Hofschneider, PH (1982). "Gene transfer into mouse lyoma cells by electroporation in high electric fields," *The EMBO Journal*. 1 (7): 841–5. doi:10.1002/j.1460-2075.1982.tb01257.x. PMID 6329708.
- [42] Electroporation: theory and methods, perspectives for drug delivery, gene therapy and research J. Gehl Department of Oncology, Herlev Hospital in University of Copenhagen, Herlev, Denmark
- [43] Martin L. Yarmush, Alexander Golberg, Gregor Sers̃a, Tadej Kotnik, and Damijan Miklavc̃ic̃, "Electroporation-Based Technologies for Medicine: Principles, Applications, and Challenges" *Annu. Rev. Biomed. Eng.* 2014. 16:295–320. DOI: 10.1146/annurev-bioeng-071813104622